To appear in Astrophysical Journal
Preprint typeset using LaTeX style emulateapj v. 08/13/06

X-RAY SELECTED AGN HOSTS ARE SIMILAR TO INACTIVE GALAXIES OUT TO $Z = 3$: RESULTS FROM CANDELS/CDF-S

D.J. Rosario[1], M. Mozena[2], S. Wuyts[1], K. Nandra[1], A. Koekemoer[3], E. McGrath[2], N. Hathi[4], A. Dekel[5], J. Donley[3], J.S. Dunlop[6], S.M. Faber[2], H. Ferguson[3], M. Giavalisco[7], N. Grogin[3], Y. Guo[7], J. Newman[8], D.D. Kocevski[2], D.C. Koo[2], R. Somerville[3]

To appear in Astrophysical Journal

ABSTRACT

We use multi-band high-resolution photometry in the 4 MSec Chandra Deep Field-South (CDF-S), in particular imaging from the Cosmic Assembly Near-IR Deep Legacy Survey (CANDELS), to explore the nuclear and extended colors, color gradients and stellar populations of X-ray selected AGN host galaxies out to z=3. Based on a study of their central light, we develop X-ray based criteria to exclude objects with strong AGN contamination. We use stellar masses from the FIREWORKS database to understand and account for stellar mass selection effects, and carefully study, for the first time, the resolved host galaxy properties of AGNs at $z \sim 2$ in the rest-frame optical light without substantial nuclear contamination. We find that AGN hosts span a large range of stellar masses, colors and color gradients at these redshifts. In terms of their colors and stellar population properties, they are very similar to inactive galaxies of the same stellar mass. At $z \sim 1$, we find a slightly narrower range in host colors compared to inactive galaxies, as well as hints of more recent star-formation. These differences are weaker or non-existent among AGN hosts at $z \sim 2$. Finally, we find that AGNs show flatter color gradients compared to inactive galaxies, with the degree of flatness correlating with AGN luminosity, implying that, even among obscured AGNs with no clear nuclear contamination, central photometry can be affected by nuclear activity, perhaps through scattered AGN light. We discuss the importance of AGN driven feedback in the quenching of galaxies at $z \gtrsim 1$ and speculate on possible evolution in the relationship between black hole accretion and the host galaxy at high redshifts.

Subject headings: galaxies: active galaxies

1. INTRODUCTION

Active Galactic Nuclei (AGNs) are associated with accretion onto super-massive black holes (SMBHs), which are generally found in the centers of massive galaxies. The high energies and unique physical environments in the vicinity of SMBHs lead to a number of characteristics properties that are displayed by AGNs: enhanced hard X-ray, mid-infrared and radio emission, high ionization and/or very broad spectral lines, rapid photometric variability. This makes AGNs relatively easy to identify, even at high redshifts.

Till quite recently, activity in galactic nuclei was studied as a topic of special interest, usually unrelated to the evolution of galaxies. This changed considerably in the last decade when tight scaling relationships were uncovered between the masses of SMBHs and the properties, especially the mass, of the spheroidal component of their host galaxies (e.g. Ferrarese & Merritt 2000; Gebhardt et al. 2000). These relationships seem to imply a close conection between the evolution of nuclear black holes and the evolution of galaxies as a whole. Such a connection is, at first glance, quite remarkable, since the typical sphere of influence of even the largest black holes is less than a few tens of parsecs in size, more than 3 orders of magnitude smaller than the typical sizes of galaxies. However, since the inflow of gas to the black hole is an essential element of SMBH growth and this depends on the circum-nuclear environment and the large-scale properties of the host galaxy (e.g., its gas content), an essential connection between black hole growth and host galaxy properties may arise through the fueling of SMBHs.

Another avenue through which nuclear activity can influence the host galaxy, despite the large difference in spatial scales, is through a set of physical processes collectively called 'feedback'. Examples include energy and momentum driven outflows in QSOs (Pounds et al. 2003), outflows accelerated by relativistic jets (Morganti et al. 2005; Rosario et al. 2010) and the suppression of cluster cooling flows by radio lobes (McNamara & Nulsen 2007).

AGN feedback can play an important role in galaxy evolution by driving and regulating the transformations of star forming galaxies into quiescent galaxies. Strong feedback form powerful AGN can eject gas from their host galaxies, effectively shutting down star-formation and moves them onto the Red Sequence. In addition, feedback can prevent gas from cooling and accreting onto these galaxies in amounts significant enough to restart star formation, thereby keeping them on the Red Sequence. AGN feedback has become an essential element of several modern semi-analytic models of galaxy formation (Bower et al. 2006; Croton et al. 2006; Somerville et al. 2008; Cattaneo et al. 2009), since it cur-

[1] Max-Planck-Institute for Extraterrestrial Physics, Garching, 85748
[2] Astronomy Department and UCO-Lick Observatory, University of California, Santa Cruz, CA 95064
[3] Space Telescope Science Institute, USA
[4] Observatories of the Carnegie Institution of Washington, USA
[5] The Hebrew University, Israel
[6] University of Edinburgh, UK
[7] University of Massachusetts, USA
[8] University of Pittsburgh, USA

tails the formation of very high-mass blue galaxies, as required by observations (Benson et al. 2003). The similarity between estimates of the time-scales of AGN activity and the quenching of star-formation also lends some credence to the relevance of AGN feedback (Bundy et al. 2008).

However, mechanisms unrelated to nuclear activity have also been proposed as drivers for the transformation of galaxies onto the Red Sequence. Most invoke the mass of the dark matter halo as a regulating factor, since the physical state of the gas that is accreted onto galaxies is influenced by virial shocks or cold flows, both of which depend on halo mass (Birnboim et al. 2007; Ceverino et al. 2010). These 'halo-quenching' models do not require AGN to play a critical role in the transformation of galaxies. The galaxy halo both suppresses star-formation and controls the growth of the SMBH by preventing the fresh inflow of gas to the disk of a massive galaxy. Currently, though, such models do not make clear predictions about the form and evolution of SMBH scaling laws.

To gauge the importance of the AGN in galaxy formation, several studies have searched for the observational consequence of AGN feedback. As yet, there is a lack of sufficient evidence for wide-spread AGN driven outflows at the level needed to satisfy the requirements of most semi-analytic models (Tadhunter 2008), except in perhaps the most powerful AGNs and in Ultra-luminous Infrared galaxies (Rupke & Veilleux 2011; Sturm et al. 2011). This may be because evolutionary models invoke a feedback prescription that is too strong, or it may be because outflows are rather transient events and difficult to characterize. An alternate approach has been to search for a direct link between the strength of nuclear activity and the transformation of the galaxy on larger scales by the examination of the structure and star-formation histories of AGN host galaxies. While indirect, these methods are more general and can be applied to the large galaxy samples across a range of redshifts.

In the local Universe, AGN tend to be preferentially in galaxies that lie between the two peaks of the bi-modal galaxy color distribution (Baldry et al. 2004; Willmer et al. 2006), i.e, they tend to hosted by so-called 'Green Valley' galaxies (Kauffmann et al. 2003; Schawinski et al. 2009). This trend is found among X-ray selected AGN even out to $z \sim 2$ (Nandra et al. 2007; Brusa et al. 2009). Galaxies in the Green Valley are generally believed to be transitioning between having significant current star-formation and being quiescent. Therefore, the over-representation of AGN in the Green Valley has been taken as evidence of the influence of AGN in the suppression of star-formation, though some doubts remain about the generality of this interpretation (Xue et al. 2010; Cardamone et al. 2010).

Morphologically, local low-luminosity AGN, such as Seyferts, are found in disk galaxies with substantial bulge components, i.e, early-type disks (Whittle 1992; Hunt & Malkan 1999; Schawinski et al. 2010). There is, however, considerable scatter in the distribution of AGN host morphologies: a large proportion, as much as 30%, have late-type spiral morphologies. Studies of the hosts of more powerful AGN suggest a similar distribution of morphological type, though with more pronounced signatures of recent galaxy mergers or interactions (Guyon et al. 2006; Bennert et al. 2008). These trends are found among AGN hosts even out to $z \sim 1$ Pierce et al. (2007); Georgakakis et al. (2009); Gabor et al. (2009) and suggest that, for the most part, low and intermediate luminosity AGN are not associated with major galaxy mergers and that secular processes may play an important role in their fueling. The case is not as clear for luminous AGN, which are rare, typically at higher redshifts and in which contamination from a nuclear point source can complicate the measurement of host galaxy structure. However, since major mergers are believed to play a critical role in the structural origin of elliptical galaxies, the frequency of post-merger signatures in QSO host galaxies may point to a close relationship between luminous phases of nuclear activity and the growth of the massive end of the Red Sequence (e.g., Hopkins et al. 2008).

Evolutionary studies of the luminosity function with redshift show that the space density of luminous AGN peaks at $z \sim 2-3$. Therefore, it is at these redshifts that one may expect the most pronounced and widespread signatures of AGN feedback on galaxy populations. Till recently, detailed studies of AGN host galaxies at these epochs have been hampered by their faintness and and the paucity of adequate samples with good redshifts. In addition, at $z > 1.5$, the 4000 Å break, a principal spectral diagnostic feature in the stellar continuum of galaxies, is redward of 1 μ. Evolved stellar populations do not emit significantly at wavelengths shortward of the 4000 Å break (or, alternatively, the Balmer break for intermediate-age stellar populations). Imaging of these distant galaxies with high-resolution instruments, such as those on the Hubble Space Telescope (HST), were generally restricted to the optical bands, which traced the rest-frame near-UV and were most sensitive to the emission from massive stars and recent star-formation. Therefore, our understanding of the structure of AGN hosts and their extended stellar populations at $z \sim 2$ were restricted to a handful of objects imaged with the second-generation HST/NICMOS camera or through Adaptive Optics instruments on large ground-based facilities.

The near-IR channel of the newly commissioned Wide-Field Camera 3 (WFC3) on the refurbished HST is greatly enchancing our view of the distant Universe by providing unprecedented sensitivity and resolution out to the H-band (approx. 1.6 μm). New surveys with the WFC3 camera are uncovering, for the first time, the stellar content of massive galaxies and AGN hosts in large enough numbers that statistical studies of their structure and stellar populations can be performed. In this study, we combine the Chandra Deep Field South (CDF-S) 4 MSec X-ray catalog with multi-band optical and NIR imaging from HST Advanced Camera for Surveys (ACS) and WFC3, as well as existing multiwavelength ground-based datasets in the GOODS-S fields. We explore resolved photometry of AGN hosts in the redshift range of $0.5 < z < 3$ and study the properties of their galaxy light without contamination from nuclear AGN emission. We derive rest-frame UV-optical colors and extinctions for these galaxies and constrain their star-formation histories (SFHs). We compare these properties to a well-defined comparison sample of inactive galaxies to place the AGN hosts in the context of field galaxy samples over the range of epochs in which most of the growth of

SMBHs and stellar mass occurs. In this way, we present an evolutionary picture of AGNs and their interrelationship with normal galaxies.

The paper is organized as follows: in Section 2, we introduce the various datasets that we bring to bear in this study; in Section 3, we discuss the selection of an AGN sample and its X-ray properties, as well as process of defining a control sample of inactive galaxies; in Section 4 and 5, we introduce the technique of aperture photometry applied to the resolved images of galaxies and the method used to derive various properties such as colors and SFHs. In Section 6, we introduce nuclear colors and define a method to remove objects where AGN light strongly contaminates the extended photometry. Finally, in Section 7, 8 and 9, we analyze the outer colors, extinctions, color gradients and star-formation histories of AGN hosts. We discuss our results in Section 10.

Throughout this work, we adopt a ΛCDM Flat cosmology with $H_0 = 72$ km s^{-1}Mpc^{-1}.

2. DATASETS

2.1. *HST imaging*

The Wide-Field Camera 3 Infra-Red Channel (WFC3-IR) is a fourth generation instrument on the HST, designed to provide low thermal background diffraction-limited imaging over a relatively wide area ($136'' \times 123''$) in the near-IR from 0.8–1.7 μm. Details of the instrument and its capabilities can be found in Baggett et al. (2008) and the WFC3 Instrument Handbook.

As part of the CANDELS Multi-Cycle Treasury Survey (Grogin et al. 2011; Koekemoer et al. 2011), a large fraction of the GOODS-S field was imaged with two NIR filters - F125W (approx. J band) and F160W (approx. H-band). The imaging dataset consists of a core set of deep exposures (part of CANDELS-Deep) and a shallower extension (CANDELS-Wide). Combined with the archival WFC3 Early Release Science (ERS2) dataset (Windhorst et al. 2011), the J and H-band imaging covers, in total, 176 arcmin^2. The CANDELS-Deep and ERS2 imaging has an average H band integration of 5 ksec, while the CANDELS-Wide extension has a depth of 1.4 ksec. The J band images have a similar depth. The individual WFC3-IR exposures were registered, cleaned and combined with a custom-built MULTIDRIZZLE-based pipeline into a single large mosaic of the GOODS-S field. Details of the survey design, depths, dither patterns, reduction, astrometric and photometric calibration, and mosaic creation can be found in the principal CANDELS reference publications (Grogin et al. 2011; Koekemoer et al. 2011). For this work, we employed the final full mosaic and its associated weightmap, rather than subsets of the images or submosaics. In addition to CANDELS WFC3 data, we also use imaging in the short Y-band filter (F098M) from the archival ERS2 program.

The imaging tiles that form the CANDELS imaging dataset were taken over multiple epochs with a range of orientations. As a result, the effective depth of the mosaic varies across its area. The mosaic weightmap takes into account the non-uniformity of the mosaic when performing photometry (§5). In practice, the exposure only changes rapidly over any particular galaxy when it lies at the boundary of one of the three principal subfields (ERS2, Deep, Wide).

We also made use of the GOODS ACS v2.0 imaging dataset, publicly available from the the online GOODS database. We downloaded image tiles in 4 optical filters (F435W, F606W, F775W and F850LP) at an average integrated exposure of 7.2, 5.4, 7.0 and 18.2 ksec in each band respectively. Descriptions of the dataset, including reductions and calibrations, can be found on the public GOODS archive and in Giavalisco et al. (2004).

The multi-epoch nature of the CANDELS dataset also produces a non-uniform Point Spread Function (PSF) across the CANDELS mosaic, as subexposures of different depth and orientation are combined at any given pixel location. Detailed modeling of stars indicate that the WFC3 PSF is quite stable across each of the subfields. This is because the WFC3 images for each epoch were generated from tiling patterns with little overlap, ensuring that submosaics from each epoch have uniform depths and most differences between the PSFs in each epoch were a consequence of the changing orientations (Grogin et al. 2011). On the other hand, the PSFs in each of the three subfields differ greatly between themselves. Therefore, we relied on a set of WFC3 PSFs derived for each of the three subfields, one for each band. These representative PSFs were constructed from model PSFs for the center of the WFC3-IR camera, generated by the TinyTim software (Hook et al. 2008), which were then drizzled together using the appropriate dither pattern for the CANDELS submosaics (Koekemoer et al. 2011). Appropriate PSFs for the GOODS ACS mosaics were created in the same way as the WFC3 mosaics. In §4, we describe how the PSFs were used to generate kernels to match the resolutions of the HST images in the different bands.

2.2. *FIREWORKS photometric database*

FIREWORKS in a K_S-band selected multiwavelength photometric catalog for the CDF-S region, with matched aperture photometry from imaging in the WFI $U_{38}BVRI$, ACS $B_{435}V_{606}i_{775}z_{850}$, ISAAC JHK_S, all four IRAC channels and MIPS 24μm bands (Wuyts et al. 2008). The catalog depth in the K_S-band is 24.3 mag (AB) and it catalog covers an area of 138 arcmin^2, overlapping considerably, but not completely, with the CANDELS GOODS-S footprint. The eastern and western edges of the ERS2 strip and a sizable wedge in the NE corner are not included in FIREWORKS, primarily because the WFC3 coverage is wider, in the EW direction, than both the GOODS-S ACS and ISAAC NIR imaging.

For the the full multiwavelength catalog, as well as details of the PSF matching, astrometric registration and photometry used to construct the catalog, we refer the reader to Wuyts et al. (2008). The FIREWORKS catalog includes photometric redshift estimates for all sources, estimated with the EAZY software package (Brammer et al. 2008). The catalog is supplemented with spectroscopic redshifts from numerous efforts in the GOODS-S field. The photometric redshifts are highly accurate, with a median offset in $(z_{spec} - z_{phot})/(1 + z_{spec})$ of 0.001, with an rms scatter of 0.032, increasing to 0.05 at $z \sim 3$. Only a few percent of objects have catastrophic redshift errors. In this work, we employ both photometric and spectroscopic redshifts from the FIREWORKS database, using the former only when the latter is unavailable. For AGNs, we also included spectroscopic

FIG. 1.— A sample of color images of representative X-ray detected AGN hosts at $z \sim 2$. The images are a combination of data in three bands: F606W in blue, F850LP in green and F160W in red, all at their native resolutions (i.e, not PSF-matched). The importance of the NIR H-band becomes obvious in these images. Most of these AGNs show weak emission in the optical ACS bands, but are well detected and bright in the H-band. In particular, the H-band traces the rest-frame optical light of the host and is less biased by strong star-forming regions, which tend to dominate the light of the hosts in the ACS images.

redshifts from more recent campaigns available in the literature (**?**).

In addition to redshifts, we adopt stellar mass estimates for galaxies based on FIREWORKS photometry and redshifts. In §5, we develop our own methodology to fit the multi-band spatially resolved SEDs of galaxies, which differs from the method used by Wuyts et al. (2008). This is because we explore the star-formation histories of galaxies in this work, which requires population synthesis modeling, while the approach in FIREWORKS is aimed primarily at deriving accurate stellar masses. Our main approach is the measurement and analysis of spatially resolved annular photometry, rather than total photometry, so we do not estimate stellar masses from our fits.

2.3. *Chandra 4 MSec X-ray catalog*

The CDF-S 4 MSec dataset consists of 54 separate exposures from the Advanced CCD Imaging Spectrometer imaging array (ACIS-I) taken between October 1999 and July 2010 as an archival resource for the community. The imaging covers an area of 464 arcmin^2 centered on $\alpha_{J2000} = 03:32:28.1$, $\delta_{J2000} = -27:48:26.0$, overlapping with the GOODS-S survey field. We reduced the CDF-S archival dataset and extracted a point source catalog from combined image. The methods used in the reduction and creation of the catalog, including the determination of PSFs, source detection and photometry, mirror those developed for the AEGIS-X survey (Laird et al. 2009). The catalog consists of 571 sources with on-axis limiting depths of 10^{-17} erg s^{-1} in the soft (0.5-2 keV) band and 1.9×10^{-17} erg/s in the hard (0.5-2 keV) band.

3. X-RAY SOURCES IN CANDELS/GOODS-S FIELD

3.1. *Near-IR counterparts of the X-ray sources*

The ACIS-I PSF varies with location on the detector and can be as large as 8" (50% encircled energy diameter) at large off-axis angles, which reduces both the spatial resolution and sensitivity to point sources for sources near the edges of the detector. This axis dependent resolution has to be taken into account when matching X-ray sources to near-IR counterparts in the FIREWORKS catalog. To do this, we adopt a Bayesian cross-matching algorithm, which takes into account the positional uncertainty of the X-ray source (which is a function of the X-ray PSF and the presence of any nearby sources), the offset of possible counterparts as well as the likelihood of a chance alignment, based on the mean number densities of sources at the K-band magnitudes of the possible counterparts. We also visually examined and verified all the cross-matches on the CANDELS H-band images, as well as removed any objects with bad imaging data.

Of the 571 X-ray sources in the 4 MSec point source catalog, 339 lie within the CANDELS NIR footprint. Of these, 304 lie in the area of the GOODS-S field covered by the ISAAC imaging and the FIREWORKS catalog. 253 sources (83%) are reliably matched to FIREWORKS counterparts highlighting the efficiency at which NIR imaging yields good counterparts to X-ray sources. This is because a substantial fraction of sources in deep X-ray catalogs are at redshifts greater than 1.5, which makes them increasing faint to optical imaging surveys, but are easily detectable in near-IR bands. Of the remaining 51 sources not matched to FIREWORKS counterparts, a major fraction appear to be associated with large bright galaxies or bright stars. The brightest galaxies in the GOODS-S field are all relatively nearby (within $z \sim 0.3$) and the detectable point-like X-ray emission may arise from either AGN activity or X-ray binaries in the outskirts of the galaxy. Since we limit our study to AGN at redshifts greater than 0.5, we ignore these low redshift X-ray sources. A small fraction appear to be associated with faint sources in the H-band images which have no FIREWORKS counterparts. These are good candidates for high redshift X-ray sources, but are beyond the scope of this work.

For the AGNs, standard photometric redshift techniques, such as those in EAZY, can yield results that are systematically in error (Salvato et al. 2009; Luo et al. 2010), due to contamination from the active nucleus. In the CDF-S, Luo et al. (2010) determine redshifts for 2 Msec X-ray point sources using a set of templates specially designed for the AGN population. We compared redshifts for sources from Luo et al. (2010) with matching FIREWORKS counterparts to 4 MSec sources. For objects where the redshifts differed by more than 0.05, we adopted the Luo et al. (2010) redshifts and recalculated stellar masses using the FIREWORKS machinery. Sources in the 4 MSec survey that are fainter than the 2 Msec depth, for which we resort to the original FIREWORKS redshifts, will be low luminosity AGNs across our range of redshifts. Standard photometric redshifts for these systems are accurate enough for our study.

In Fig. 2, we plot the FIREWORKS K_s magnitude of the cross-matched X-ray sources as a function of redshift and compare them to the distribution of all galaxies in the FIREWORKS catalog. Objects with spectroscopic redshifts are shown as large red circles, while objects with photometric redshifts are marked as large green circles. From the Figure, it is clear that the X-ray sources tend to be among the brightest objects at any given redshift. This implies that X-ray AGN are generally found in hosts that are luminous and relatively massive, as shown in many previous studies (e.g, Nandra et al. 2007; Brusa et al. 2009).

At $z < 1.5$, the majority of X-ray source counterparts have redshifts that are determined through spectroscopic methods and are highly reliable. An increasingly larger fraction of sources at $z > 1.5$ have photometric redshifts. As mentioned before, FIREWORKS has a small normalized rms redshift error even at these higher redshifts, as well as a small catastrophic error rate of around 3%. Such small errors in the photometric redshifts should not introduce any significant systematic biases in the SED fits or color trends described later in this work, as shown by our tests of the effects of redshift errors on the color distributions of galaxies in §6.2. For our purposes, we treat both spectroscopic and photometric redshifts equivalently in the following discussions.

For this study, we restrict ourselves to galaxies with redshifts between 0.5 and 2.8, indicated in Fig. 2 with dashed vertical lines. The low end of this range marks the redshift at which a substantial fraction of X-ray sources have their X-ray emission coming primarily from star-formation or weak AGN activity ($L_{2\text{-}10} < 10^{42}$ erg s^{-1}). The upper end of the range is the redshift at which the rest-frame 4000 Å break enters the observed H-band (the

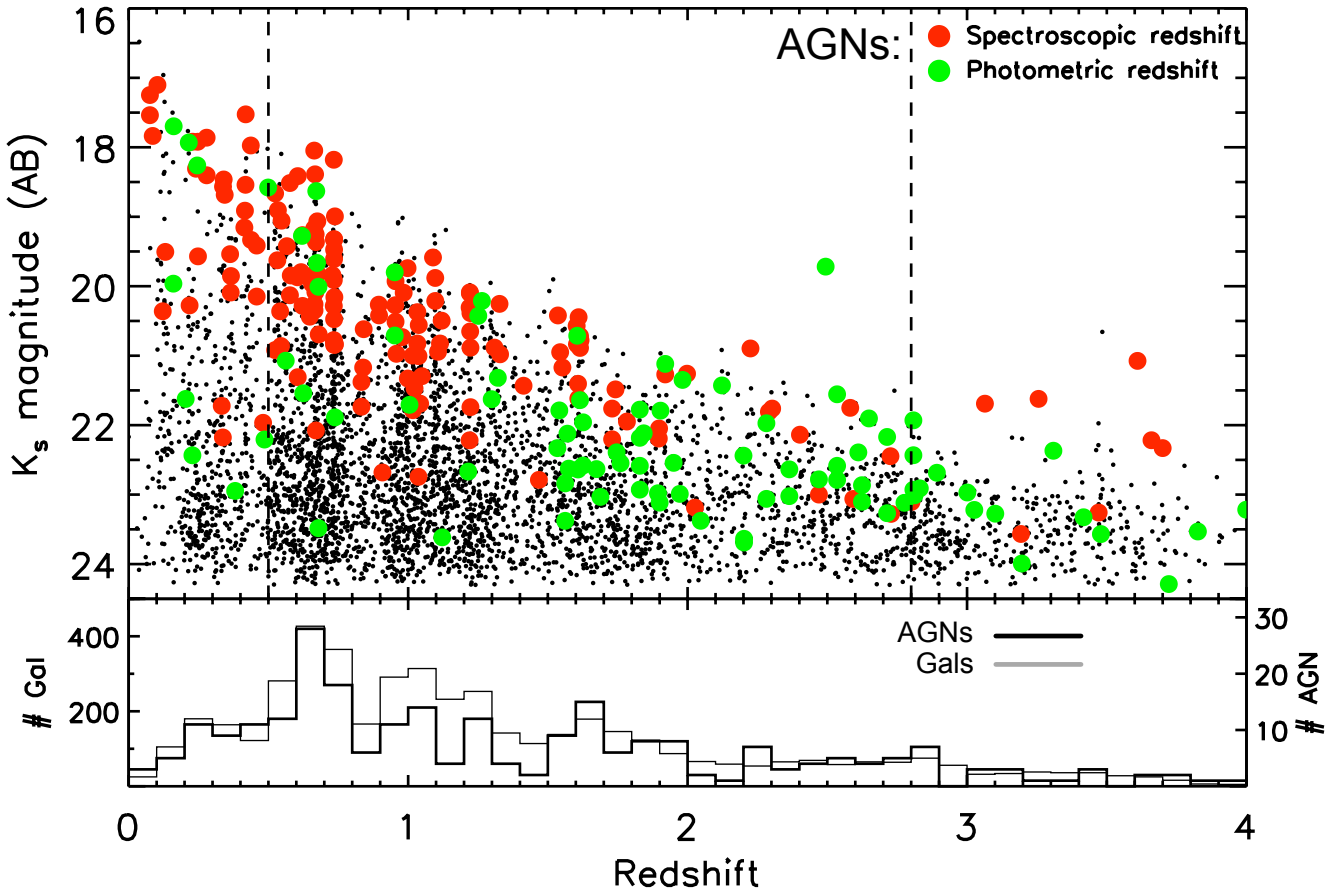

FIG. 2.— Apparent K_s magnitude plotted against redshift for X-ray sources detected in the CDF-S 4 Msec dataset (large points), as well as normal X-ray undetected galaxies from the FIREWORKS catalog (small points). The red points are X-ray sources with a counterpart with a spectroscopic redshift, while the green points are sources with a photometric redshift. The histograms in the lower panel plots the redshift distribution of the FIREWORKS galaxies (thin line, left Y-axis) and the AGNs (thick line, right Y-axis). The dashed lines mark the redshift range to which we restrict this study ($0.5 < z < 2.8$).

reddest band we consider for aperture photometry). At wavelengths bluer than the 4000 Å break, light from young stars can greatly dominate the galaxy SED, but not its total stellar content. We restrict our sample to redshifts in which the H-band traces light from the bulk of a galaxy's stars.

Applying our redshifts cuts and requiring coverage in all four GOODS v2.0 optical bands yields a final sample of 176 X-ray sources. Of these, 70 lie in the redshift range 1.5–2.8. This is by far the largest sample of normal high redshift AGNs studied at rest-frame optical wavelengths.

3.2. *X-ray luminosities and hardness ratios*

The multi-band X-ray count rates and FIREWORKS redshifts are used to estimate rest-frame X-ray luminosities and obscuration in our working sample of X-ray sources. We assume that all sources have an intrinsic power-law spectrum at X-ray wavelengths with a photon index of $\Gamma = 1.9$ (Nandra & Pounds 1994). We simultaneously fit the fluxes in the observed-frame full (0.5-10 keV), soft (0.5-2 keV), hard (2-10 keV) and ultra-hard (4-10 keV) X-ray bands, corrected for Galactic absorption, to estimate the intervening Hydrogen column density (N_H), using the photoelectric crossections of Morrison & McCammon (1983). These fits are used to derive intrinsic (de-absorbed) hard X-ray luminosities

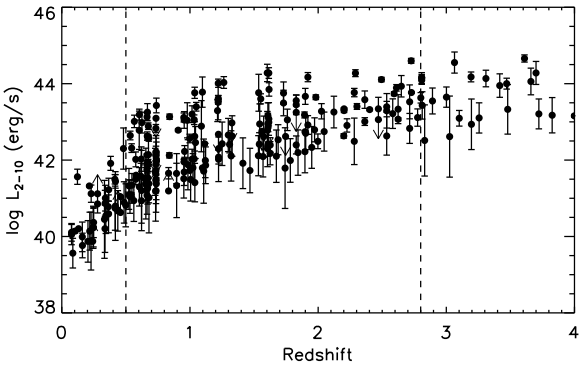

FIG. 3.— Rest-frame X-ray luminosity in the hard band (2-10 keV) vs. redshift of CDF-S X-ray sources with FIREWORKS counterparts.

$L_{2\text{-}10}$ in the rest-frame 2-10 keV band.

In Fig. 3, we plot $L_{2\text{-}10}$ against redshift for our sample. For sources in which the N_H estimate is greater/lesser than the upper/lower allowed bound (log N_H = 25/19 cm^{-2}), we set an lower/upper limit to $L_{2\text{-}10}$. Only 9 sources of 176 give limits, typically because they are detected in only a single X-ray band. We disregard sources with limits in our general analysis. Galaxies with

$L_{2\text{-}10} < 10^{42}$ erg s^{-1} can possibly be contaminated by X-ray emission from star formation and stellar remnants (refs). Therefore, we set this luminosity limit as a minimum criterion for an X-ray source to be a pure AGN. The application of these two criteria excludes 58 objects, leaving us with a final working sample of 118 bona fide AGN spanning a redshift range of 0.5–2.8 and almost 3 orders of magnitude in X-ray luminosity.

The de-absorbed X-ray luminosity is generally quite robust to the exact parameters of the X-ray fits, since for most of our redshift range, the rest-frame 2-10 keV band is bracketed by the soft and hard bands in the observed frame. In addition, the optical depth to photoelectric absorption in the hard band is low for typical obscuring columns in X-ray selected AGNs. However, the value of N_H is generally more uncertain and has systematic variations with redshift, as the obscuration-sensitive rest-frame soft band is redshifted out of the Chandra/ACIS band-pass. In particular, higher redshift AGNs will have systematically higher N_H.

In Fig. 4, we plot the X-ray luminosity ($L_{2\text{-}10}$) of the AGNs against the FIREWORKS stellar mass of the host galaxy. If any direct relationships exist between AGN luminosity (or accretion rate) and the host galaxy mass – say, if black holes in low-mass galaxies have very different Eddington ratio distributions from high-mass galaxies – we can constrain them in this diagram. As the range of X-ray luminosity of the AGN sample changes with redshift (Fig. 3) due to the flux-limited depth of the 4 Msec dataset, any such trends could translate into an apparent evolution of host galaxy properties with redshift.

In both redshift bins in this plot, there is a general lack of any relationship between $L_{2\text{-}10}$ and stellar mass. At any given galaxy mass (and, by extension, black hole mass), there exists a wide range of AGN luminosity. However, a small number of low mass galaxies ($M_* \lesssim 10.0$) are found to be associated with X-ray sources, and they host AGNs with a lower average luminosity than the general population of more massive galaxies. These objects are probably due to a tail of lower mass black holes with large Eddington ratios, bringing them into our flux-limited AGN sample.

AGNs with strong signs of nuclear contamination (marked with concentric circle points; see §6) tend to have slightly lower stellar masses compared to the bulk of the AGN sample. This is because population synthesis methods, such as those used in FIREWORKS to derive stellar masses, typically fit young populations to these objects to match their blue AGN-contaminated colors. The M/L ratios of such populations are low, resulting in incorrectly low stellar masses.

3.3. *Control sample*

The main goal of this work is to explore the nature of the host galaxies of AGN at high redshifts. In order to fully understand AGN hosts, they must be placed within the context of the normal field galaxy population at comparable epochs. Many studies have shown that there has been substantial evolution in the properties of normal galaxies since $z \sim 3$: the star-formation rate at a given stellar mass has decreased by an order of magnitude (Noeske et al. 2007; Tresse et al. 2007), the space density and stellar mass of red galaxies has increased by a similar amount (Arnouts et al. 2007; Taylor et al. 2009) and stellar mass functions of galaxies show considerable evolution, especially at the low-mass end (Marchesini et al. 2009). In addition, these studies also demonstrate considerable correlation of galaxy properties with stellar mass. We control for these transformations and variations by defining two sets of normal galaxies, to which we compare the properties of AGNs throughout this paper. The first set is a representative sample of inactive galaxies with masses and luminosities comparable to the AGNs. The second is a refined sample with a stellar mass distribution that is matched to the AGNs.

To define our control samples, we first identified the range of stellar mass and rest-frame B-band absolute magnitude (M_B) that AGNs occupy across our redshift range of interest. Using rest-frame photometry and stellar masses from the FIREWORKS catalog, we find that essentially all AGNs that are matched to FIREWORKS counterparts lie in galaxies that have a stellar mass log $M_* > 9.3$ $M_\odot$ and $M_B < -19.5$. Therefore, we examined the images of all FIREWORKS galaxies without X-ray detections in the redshift range $0.5 < z < 2.8$ which satisfy these limits in stellar mass and M_B. We excluded any that did not have images in the WFC3 J/H bands and the four GOODS ACS bands, as well as a few that lay too close to the edges of the ACS and WFC3 mosaics, or those with image defects or contamination from bright nearby stars or galaxies. This leaves us with a high quality set of 1683 inactive galaxies with a similar range of luminosity, mass and multi-wavelength coverage as the AGNs in our sample. The redshift distribution of these galaxies, hereafter called the 'general control sample', is similar to that of the AGNs (lower panel of Fig. 2).

From the general control sample, we applied a further selection to get a 'mass-matched control sample'. First, we divided the AGNs and normal galaxies by redshift into the same redshift bins as those used in our subsequent comparative study (see later sections). For each AGN in a bin, we randomly chose three distinct normal galaxies in the same redshift bin with a stellar mass within 0.2 dex of the AGN's mass. The factor of three is a balance between a sufficient sized sample of control galaxies for significant statistics and the need to closely match the mass distribution of the AGNs, especially at high masses, at which the AGN fraction among galaxies can be quite large at $z \sim 2$.

At intermediate to high AGN luminosities, contamination of optical and IR light by the emission from the active nucleus can systematically alter stellar mass estimates for AGN hosts, as shown in Fig. 4. In the next section, we outline a method to exclude AGNs with the strongest contamination, using a combination of X-ray luminosity and obscuration cuts. These cuts only affects a small fraction of objects (9%). For most AGNs in our sample, the effects of contamination are minimal and do not significantly bias our control sample selections.

In Fig. 5, we compare the stellar mass distributions of the two control samples with the AGNs in three redshift bins: 0.8–1.2, 1.2–2.0 and 2.0–2.8. These three bins will be used frequently in the rest of this work and we call the, for brevity, the 'low', 'intermediate' and 'high' bins respectively. Keep in mind that low and high bins here cover redshifts $z \approx 1$ and $z \gtrsim 2$, not 'low' and 'high' redshifts in the sense of the standard literature (which usually mean local and $z > 4$/dropout samples respec-

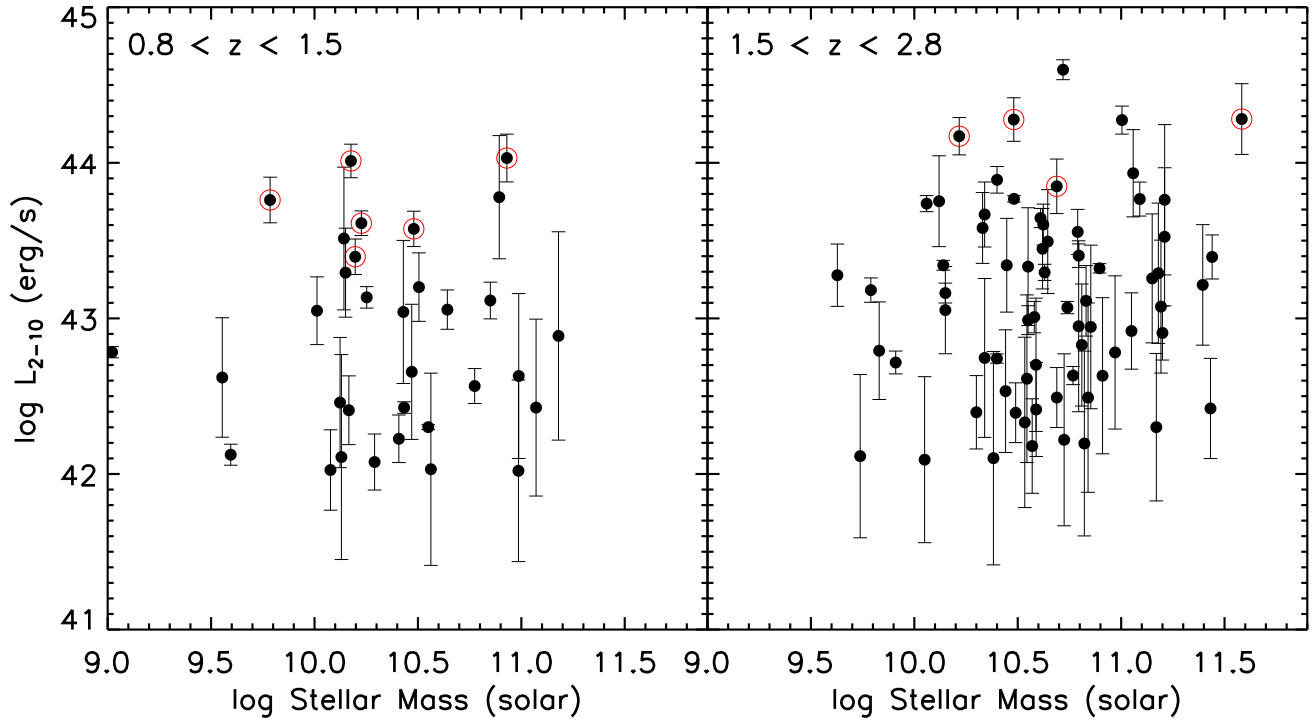

FIG. 4.— Hard band X-ray luminosity ($L_{2\text{-}10}$) against stellar mass for AGNs in two redshift bins. Objects with strong nuclear contamination have been removed from this plot, since their stellar masses are likely to be incorrect. Note the lack of any obvious correlation, though a tail of low mass galaxies with low X-ray luminosities can be seen in the low redshift bin.

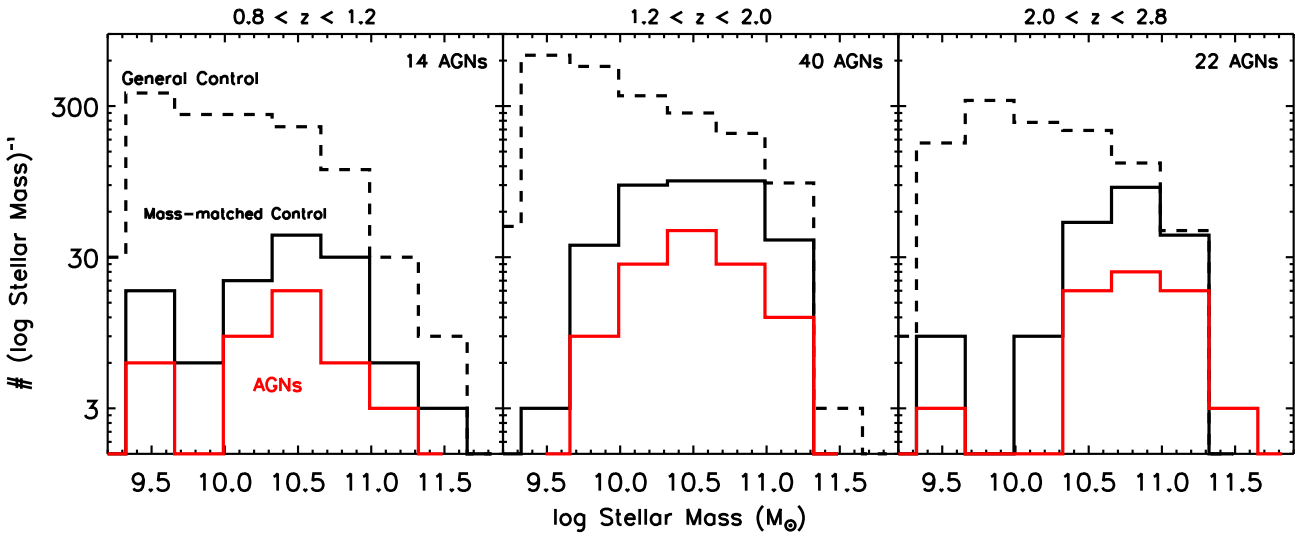

FIG. 5.— Stellar Mass (M_*) distributions of AGNs (red solid lines) compared to the general control sample (dashed lines) and the mass-matched control sample (black solid lines) in three redshift bins. The AGNs (and mass-matched control galaxies) tend to be more massive than the field galaxy population.

tively). AGNs with substantial nuclear contamination have been excluded from this plot.

The general control sample has a distribution (dashed line) that is approximately Schecter-like, while that of the AGNs and mass-matched control sample (red and black solid lines) drop-off strongly towards low masses. A close correspondence between the red and black solid lines highlights the quality of our mass-matching procedure.

AGNs are weighted towards being found in rather massive galaxies. The peak in the AGN mass distribution is at $\log M_* \approx 10.5 - 10.7$, increasing slightly with redshift. In addition, the fraction of massive galaxies hosting AGNs increases drastically with redshift. While AGNs are only a few percent of similar mass galaxies in the low bin, the fraction increases to more than 30% at the high mass end in the high bin.

The typical stellar masses of the AGN hosts are much higher than the mass incompleteness limit of the FIRE-WORKS catalog at all redshifts. Since there is no trend of AGN luminosity with stellar mass (Fig. 4), this implies that the slight evolution in the peak mass is proba-

bly real and not a consequence of differences in the AGN luminosity range with redshift. It may be related to the strong increase in the space density of AGNs. A detailed look at mass functions of AGNs is beyond the scope of this paper, but we discuss some aspects of the evolution of the AGN mass function in §10.

4. APERTURE PHOTOMETRY

For each galaxy in our AGN and control samples, we performed aperture photometry on the full set of seven HST images, 4 ACS/GOODS and 2-3 WFC3/CANDELS bands. Several steps of data preparation were needed before the final photometric measurements.

We first used the PSFMATCH routine within IRAF [9] to develop convolution kernels to match the PSFs of the images in all bands to those of the H-band. This was done separately in all three subfields. Despite the high quality of our model PSFs, some residual high-frequency noise remained, which we removed by applying a cosine-bell apodizing function to the Fourier transform of the PSFs. The psf-matching procedure reproduces the extended structure of the H-band PSF very accurately in all the GOODS and WFC3 images. However, the core flux of the H-band PSFs differed from the psf-matched versions at the level of 10%, primarily due to the low-pass filtering of the PSFs. This yielded simulated PSFs that had slightly broader cores than that in the H-band (by 15-20%, depending on the width of the original PSF). Photometry of galaxies in apertures with sizes close to that of the WFC3 H-band PSF (such as the 'nuclear' aperture used in later sections) yield SEDs that are slightly too red, as some of the light in the core of the bluer bands is scattered out of the aperture by the PSF-matching process. The degree to which this effect operates is a strong function of the compactness of the galaxy image. However, since we compare AGNs to inactive galaxies, in practice this 'PSF-reddening' will not significantly affect our results, as long as it influences both sets of galaxies equivalently.

A peak-up centroid of the WFC3 H-band image of the galaxy was measured for each object, using the IDL routine GCNTRD. The coordinates of this centroid was used as the fixed center of all photometric apertures in all the images of the galaxy. Despite its lower diffraction-limited resolution compared to the ACS images, the H-band image was used to measure the center of light because it is the longest wavelength HST band. This ensures that the diffuse stellar light of the galaxy has the most contrast over light from a nuclear point source or from star-forming knots. In addition, for most sources with $z > 2$, the galaxy itself is quite faint or barely detected in the short-wavelength ACS images.

After convolving the images in each band to bring them to a common H-band PSF, we used the IDL program APER to measure counts in a set of annular apertures, ranging from $0\farcs1$ to 4", centered on the coordinates of the the H-band centroid. The photometric measurements were converted to AB magnitudes using standard zero-points from the GOODS v2.0 (Giavalisco et al. 2004) documentation for the ACS images and the WFC3 documentation on the instrument webpages at the Space Telescope Science Institute. Since the images used for the photometry were brought to the same PSF and we only require that the relative flux across bands in each aperture remain accurate, we did not apply any aperture corrections to our photometry, but instead applied these zero-points directly to the total counts that were measured. Errors were estimated from the multidrizzle weight maps, with a standard correction for correlated pixel-to-pixel noise.

[9] Image Reduction and Analysis Facility, distributed by the National Optical Astronomy Observatory

5. MODEL FITS AND STATISTICS

5.1. *SED Fitting and Parameter Estimation*

The main thrust of this paper is to self-consistently study rest-frame properties (colors, mean extinctions) and the stellar populations (ages, SFHs) of X-ray selected AGN hosts across redshift, and compare them to the properties of inactive galaxies. Towards these ends, we employ a library of synthetic SEDs derived from the population synthesis models of Maraston (2005). Starting with a set of Single Stellar Populations (SSPs) with metallicities of 1/2, 1 and 2 times solar, we generated models with three possible star-formation histories (SFHs) – constant star-formation, exponentially decaying star-formation (negative 'τ-models') and exponentially *increasing* star-formation (positive 'τ-models'). The latter set of models are rarely employed in studies to date, but recent work suggests that SFHs that increase with time may be more relevant at $z \gtrsim 2$, since the mean star-formation rate density of the Universe turns over at that epoch (Maraston et al. 2010). Therefore, we consider both increasing and decreasing models in this study. The star-formation history is parameterized by a finely sampled set of 43 ages (since the onset of star-formation), ranging from 0.01 to 15 Gyrs, and 16 exponential timescales (τ), ranging from 0.05 to 20 Gyr. In addition, we applied a foreground-screen dust reddening prescription with a Calzetti reddening law (Calzetti et al. 1994), parametrized by the visual extinction A_V in 16 uniformly logarithmic steps from 0.001 to 7. We derived model magnitudes for each SED at a set of redshifts between 0.4 and 4.0, with uniform steps in redshift of 0.01. At any redshift, only models that were younger than the age of the Universe were considered. Magnitudes were evaluated in the observed frame for the 7 HST bands, ISAAC K_S and the four IRAC bands, using the most up-to-date filter functions publicly available. Our library of model SEDs is sufficient to capture the bulk of spectral variation among galaxies, verified by comparing the empirical range of rest-frame colors among galaxies in the FIRE-WORKS catalog with that of our model set.

For each galaxy (AGN host or control) and a given annular aperture, we fit for a scaling parameter that minimized the χ^2 difference between the model and measured fluxes, at a grid redshift closest to the measured redshift of the galaxy. This minimum χ^2 for the model was then stored. In this way, we obtained a four-dimensional χ^2 space for each galaxy, parametrized by SFH model (constant/range of positive and negative τ), age, A_V and metallicity. We applied an additional constraint that the synthesized K_S and IRAC magnitudes for any model fit to the SED of an annular aperture must be less than the total measured K_S and IRAC magnitudes of the galaxy, up to a rest-frame wavelength of 1.6μ. In practice, this constraint only excludes the most dusty models at the

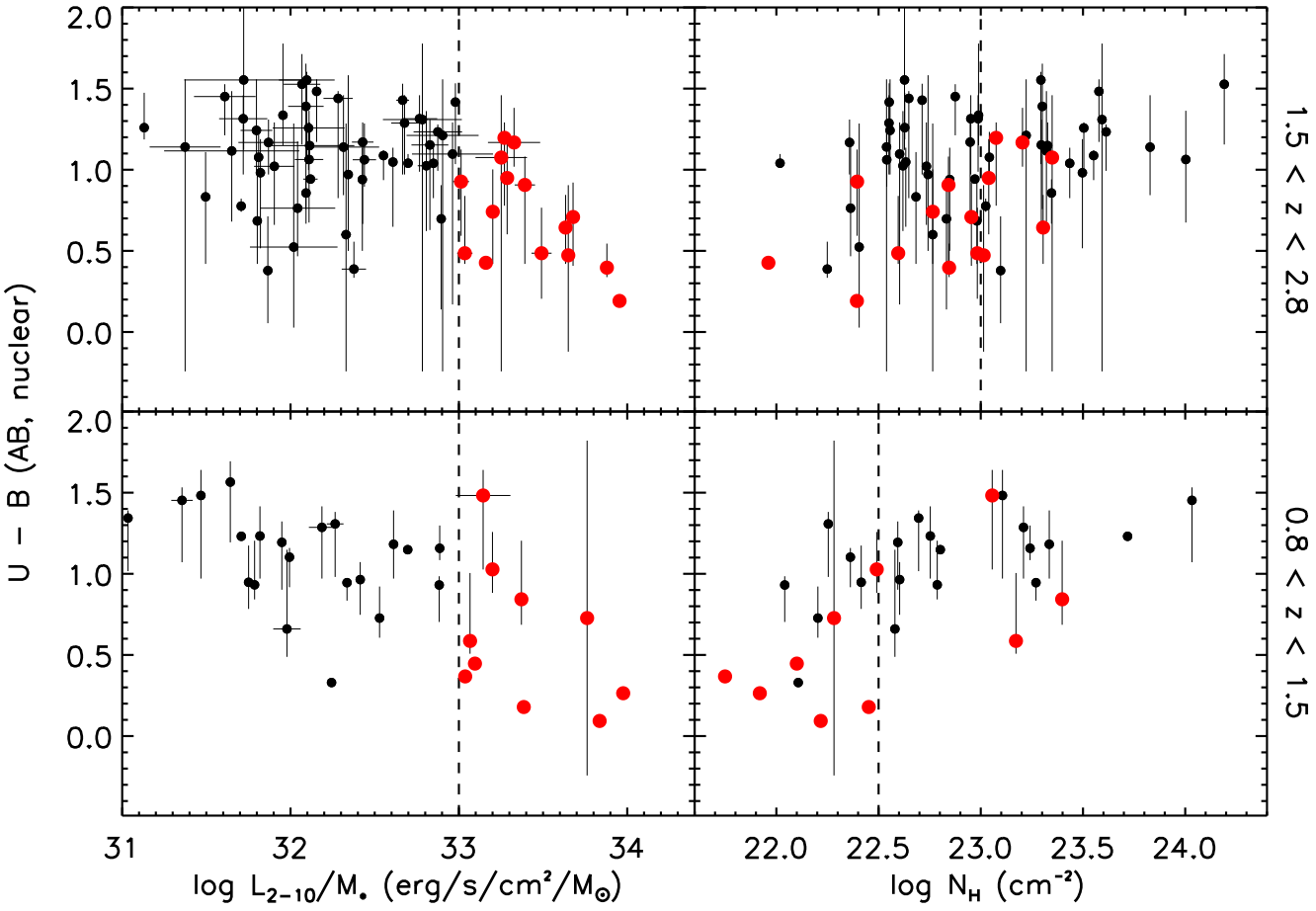

FIG. 6.— The rest-frame nuclear U-B colors of AGN hosts plotted against the ratio of hard-band X-ray luminosity to stellar mass (left panels) and the Hydrogen column density of X-ray obscuring gas N_H (right panels). The lower panels show AGNs at intermediate redshifts ($0.8 < z < 1.5$), while the upper panels show AGNs at high redshifts ($1.5 < z < 2.8$). The vertical dotted line in the left panels mark the transition value of $L_{2\text{-}10}/M_*$ beyond which nuclear emission from the AGN prominently affects the nuclear colors. These sources are marked as red points in all panels and appear to separate out in the plane of color vs. N_H. The blue sources are generally soft, while the red sources are typically harder, which high values of N_H. The dotted vertical lines in the right panels mark the values of N_H used in combination with the transition $L_{2\text{-}10}/M_*$ to separate out sources with nuclear contamination

highest redshifts, but is included for physical consistency.

From this χ^2 space, we developed a method to derive the best-fit value and accurate confidence intervals for any model-dependent parameter (age, *tau*, rest-frame colors, A_V), similar to the procedure described in Salim et al. (2005) for population fits to galaxies SED from UV-to-IR SEDs. Consider, as an example, the rest-frame U-B color of the galaxy. We concentrate on this color since it is uniquely sensitive to the mean light-weighted stellar population of a galaxy, since the two bands constituting the color lie of either side of the 4000 Å break. Each model has a particular value of rest-frame U-B, calculated directly from its synthetic spectrum. The best-fit value of U-B corresponds to the model with the lowest χ^2 value. The uncertainty in U-B is given by the minimum and maximum color of all models that deviate from the lowest χ^2 by less than 3.5, which defines the appropriate 68% (1σ) confidence interval for three degrees of freedom (7 bands - 4 model parameters). The advantage of using the full χ^2 space is that systematic uncertainties due to degeneracies in the model space, which can frequently be larger than purely statistical uncertainties, are taken into account in this method.

In this way, we arrive at best-fit values and confidence intervals for observed and intrinsic rest-frame colors, visual extinction, stellar age, τ and the ratio of stellar age over τ (the 'normalized age') for each galaxy. The last two quantities are only appropriate for galaxies fit with τ models.

5.2. *Monte-Carlo Bootstrapped Distributions*

A important part of the following analysis involves comparing distributions of various estimated quantities (colors, SFH parameters) between AGNs and inactive control galaxies. The small size of the sample and the large uncertainties on some of the parameters from the SED fitting analysis makes interpretation of any differences in the distributions of best-fit parameters rather difficult. As the library of models do not uniformly sample parameter space, best-fit values of a parameter can be over-represented in regions of parameter space that are more well-sampled than others.

To enable a reasonable comparison to be made between

FIG. 7.— Three-color VzH images of the sixteen AGNs in the redshift range $0.8 < z < 2.8$ which have been flagged as galaxies with strong nuclear AGN contamination, based on X-ray based criteria (§6). Bright blue nuclear point sources are seen in almost all these sources.

the parameter distributions of AGNs and control galaxies, we developed a two step monte-carlo bootstrap approach to arrive at more representative distributions for both samples. For each object, we take the best-fit parameter from the SED fits to be a median value. We randomly vary the parameter about this value taking the upper and lower 1σ confidence intervals as the standard deviations of a two-sided piece-wise gaussian probability distribution, where the probability of a random deviate being positive or negative is 0.5 (by construction, as the best-fit value is assumed to be a median value). For some parameters, such as stellar age, we apply upper and lower bounds to the random deviate consistent with any limits enforced in the SED fitting process. This process is repeated 1000 times per object. The final distribution in each redshift bin is derived from the entire simulated set of parameters for all objects (AGNs or control) in that bin. We term this bootstrapping step 'Loop 1'. While Loop 1 takes into account the uncertainties that come out of the SED fitting process, it does not consider the effects of the limited sample size of the AGNs – stochastic effects can play a big role in the shape of a parameter distribution. To account for this, we run Loop 1 on a subsample of N randomly chosen galaxies from the control sample in a redshift bin, where N is the number of AGNs in the same redshift bin. This second set of monte-carlo simulations is called 'Loop 2' and it allows us to place upper and lower 1σ uncertainties on the distribution of the control galaxies resulting from stochastic effects from the small size of the AGN sample in any given bin. The distributions of AGNs and control galaxies are only significantly different if they have consistent offsets that are larger than the 1σ errors bars on the control galaxy distributions. Note, however, that this process does not regularize stochastic variations due to the limited sample size of the control galaxies. In all redshift bins, the mass-matched control galaxy samples range between 45–110 objects, and the general control sample, of course, is much larger. Therefore, stochastic effects among these galaxies should be small. However, we have checked the validity of our main results through several iterations of the mass-matching procedure described in §3.3. All our conclusions are unchanged in several randomly different mass-matched control samples.

6. NUCLEAR COLORS AND OBSCURATION

The active nucleus is a source of considerable high-energy radiation. In cases where the emission from the AGN is relatively unobscured to optical light, the nucleus can appear as a point-source in galaxy images, frequently blue in color. The high spatial resolution of the WFC3 NIR images allows a better characterization of the SED of the nuclear light in AGNs at $z \sim 1$ and allows us to constrain the contribution of non-stellar emission to the nuclear light in AGNs at $z \sim 2$ more accurately than ever before.

The degree to which light from an unobscured active nucleus can contaminate the light of a galaxy is a direct function of the luminosity of the AGN and an inverse function stellar luminosity of the galaxy. To account for both dependencies, we construct a parameter $L_{2\text{-}10}/M_*$ which is the ratio of the X-ray luminosity of an AGN to this stellar mass of its host.

In Fig. 6, we plot the rest-frame 'nuclear' U-B color of the X-ray AGNs against $L_{2\text{-}10}/M_*$ (left panels) and the X-ray obscuring hydrogen column density N_H (right panels). The 'nuclear' photometry is estimated within a central circular aperture $0\farcs2$ in diameter, corresponding to a physical scale of ≈ 1 kpc across our redshift range of interest. The aperture size is larger than the $0\farcs15$ FWHM of the WFC3 H-band PSF and encloses $\approx 40\%$ of any unresolved central light. We separate the AGNs into two redshift bins in this plot: $0.8 < z < 1.5$ and $1.5 < z < 2.8$.

The nuclear colors of AGNs at $0.8 < z < 1.5$ are predominantly redder than U-B = 0.8 (approximately the top of the Blue Cloud at these redshifts – see §7.3.1). However, above a transition value of $\log L_{2\text{-}10}/M_* = 33$ erg $s^{-1}M_\odot^{-1}$ (red points), some AGNs show scatter towards much bluer nuclear colors. In addition, the blue color appears to correlate with $L_{2\text{-}10}/M_*$, suggesting that the excess blue light in the centers of these AGNs comes from nuclear emission. Indeed, a visual inspection of these bright AGNs with blue nuclei clearly show nuclear point sources (Fig. 7). Most also have broad AGN lines visible in their spectra (**?**).

The right panels allow us to compare the X-ray obscuration properties of the AGNs as a function of nuclear color. In the lower right panel, the red and blue branches of the bright AGNs (red points) separate out in N_H. Objects with blue colors all show relatively low obscuration ($\log N_H \sim 22$), while those with red colors show a larger range in N_H, but tend to be higher. In other words, luminous AGNs that are unobscured towards the nucleus in optical light are also relatively unobscured at X-ray wavelengths, while those that are obscured at optical wavelengths generally show a larger X-ray obscuration as well.

The anti-correlation between visible nuclear optical emission and the level of X-ray obscuration has been noted in previous work on AGN host color gradients, typically at $z \sim 1$ (Pierce et al. 2010). The simplest interpretation of this trend is the existence of a relationship between the medium that obscures the optical light of the AGN accretion disk and the medium that obscures the X-ray emission.

A similar behavior is seen at high redshifts (top left and right panels), with some qualitative differences. The colors of the unobscured AGNs are not as blue as at lower redshifts. This could be because the optical obscuration towards the nucleus at $z \sim 2$ is larger on average compared to that at $z \sim 1$, since the gas fraction of galaxies increases towards high redshifts. Another possibility is that the fraction of stellar light within the nuclear aperture is larger at $z \sim 2$, as galaxies at these redshifts are generally quite compact. This will reduce the contrast of AGN emission against that of the galaxy.

In addition, the mean N_H between the AGNs with blue and red nuclear colors is not as pronounced at $z \sim 2$ as at intermediate redshifts. This difference is hard to interpret accurately, since the X-ray spectral fit param-

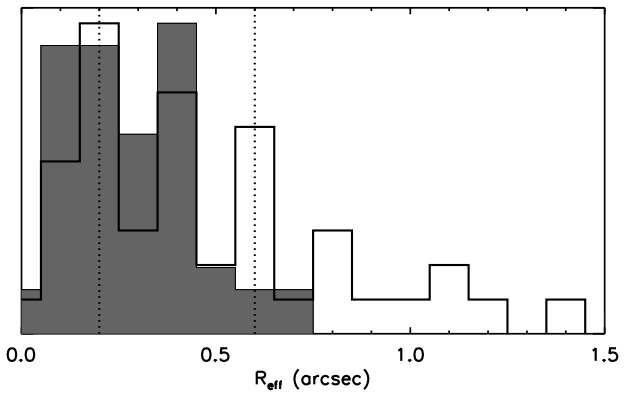

FIG. 8.— Histograms showing the distribution of effective radii R_{eff}, in arcseconds, of non-active galaxies at $0.8 < z < 1.0$ (unfilled histogram) and $2.0 < z < 2.5$ (filled histogram). The dashed lines show the inner and outer radii of the circular annulus that is used for the study of outer colors in §7.2.

eters, and especially N_H, can vary systematically with redshift. If true, it may represent a gradual change in the relationship between optical and X-ray obscuration towards higher redshifts. For example, at $z \sim 1$ optical obscuration could come primarily from dusty gas in the vicinity of the SMBH, such as the putative dusty torus which is invoked in Unification schemes for local AGNs (Antonucci 1993). However, at $z \sim 2$, more of the optical obscuration may arise from intervening dust within the gas-rich ISM of the host galaxy. In both cases, most of the X-ray obscuration probably arises in very dense gas surrounding the AGNs accretion disk, since the typical column densities of galaxy disks cannot account for the high values of N_H.

We are now able to decide on criteria to allow us to flag and remove AGNs with likely strong nuclear point sources from the following analysis of outer colors and star-formation histories. Since nuclear colors can be blue due to both AGN emission or strong star-formation, we choose not to use pure color criteria, since this can remove galaxies with genuine nuclear star-formation, rather than strong AGN activity. Instead, we employ purely X-ray based criteria. We decide on log $\log L_{2\text{-}10}/M_* = 33$ erg $s^{-1}M_\odot^{-1}$ and log $N_H < 22.5/22.9$ cm^{-2} at z lesser/greater than 1.5, guided by the results of Fig 6. In Fig. 4 and 9, these AGNs with nuclear contamination are marked with concentric circle points.

7. HOST GALAXY COLORS

In this section, we study the rest-frame U-B color of the AGN hosts in annular apertures that are relatively free of nuclear contamination, and compare them to the rest-frame U-B color of various control galaxy samples across various redshift bins.

7.1. *Choice of Working Annulus*

In this study of extended light, we will work in an annular aperture of fixed angular size across all redshifts. This is preferred over working with apertures of fixed physical size for two primary reasons:
a.) Any comparison of photometric properties between annular apertures of different sizes will need to take into account the smearing effects of the PSF, which is dependent on the light profile of the galaxy, strength of nuclear AGN emission and the radius of the annular aperture. These effects can be hard to model *a priori* and may have considerably uncertainties and systematics. However, working in fixed annular apertures at all bands and redshifts keeps these effects fixed as well, and greatly simplifies the interpretation of any comparisons.
b.) The angular diameter distance scale varies by less than 15% between the redshifts of 0.8 and 3 and only by about 30% between redshifts of 0.5 and 1. Therefore, a comparison of outer colors of galaxies between $z \sim 1$ and $z \sim 2$ at fixed angular apertures is essentially equivalent to a comparison at fixed physical apertures.

To arrive at an optimal annular aperture to study the extended light of AGN hosts, we perform light profile fits to the z-band and H-band images of inactive galaxies in the ERS2 region of the CANDELS/GOODS-S field. We concentrate on two sets of galaxies, subsets of the mass-matched control sample in the redshift ranges $0.8 < z < 1.0$ and $2.0 < z < 2.5$. The z-band and H-band cover a similar range of rest-frame wavelengths at the lower and higher redshift bin respectively, which makes it possible to compare their sizes without the complications of a structural k-correction. We model the galaxies using the GALFIT code (Peng et al. 2010) as two-dimensional elliptical sersic profiles, with sersic indices in the range of 0.5-6 and effective radii left free.

The distribution in R_{eff} for non-active galaxies at $0.8 < z < 1.0$ (from z-band images - unfilled histogram) and $2.0 < z < 2.5$ (from H-band images - filled histogram) is shown in Fig.8. Both sets of galaxies have modal sizes around $0\farcs3$ (2.4/2.5 kpc across at redshift 1/2.2), though those at lower redshifts have a substantial tail towards larger sizes while most distant galaxies have R_{eff} smaller than $0\farcs5$. We choose an outer annular radius of 1", which encompasses most of the light of galaxies across our redshift range of interest. The inner radius of the annulus has to be large enough to minimize contamination from the central light of the galaxy (nuclear or stellar), so that valid measure of color gradients can be made. After experimenting with the relative size of the H-band PSF and various aperture sizes, we settled on an inner aperture of 0.4". Beyond this radius, the extended light in the smaller galaxies is contaminated by unresolved central emission at the level of a few–10%, and even less for the larger galaxies. The inner and outer annular radii are marked in Fig.8 with dotted lines.

Having said this, nuclear continuum emission in bright AGN can still substantially affect the extended light aperture at blue and UV wavelengths, which will skew our SED fits towards bluer colors and younger mean ages. Therefore, we also employ the criteria based on our study of nuclear colors to remove the small fraction of AGNs with strong nuclear point sources.

7.2. *Outer Colors and AGN Properties*

In parallel to what was done in §6, we plot, in Fig. 9, the outer U-B color of AGN host galaxies against hard-band X-ray luminosity (left panels) and Hydrogen column density to the nucleus (right panels), to search for relationships between nuclear activity, X-ray obscuration and the properties of the host stellar populations. In this figure, we include with luminous, soft X-ray sources, marked with concentric circle points. The galaxies typically show quite blue colors due to the bright nuclear

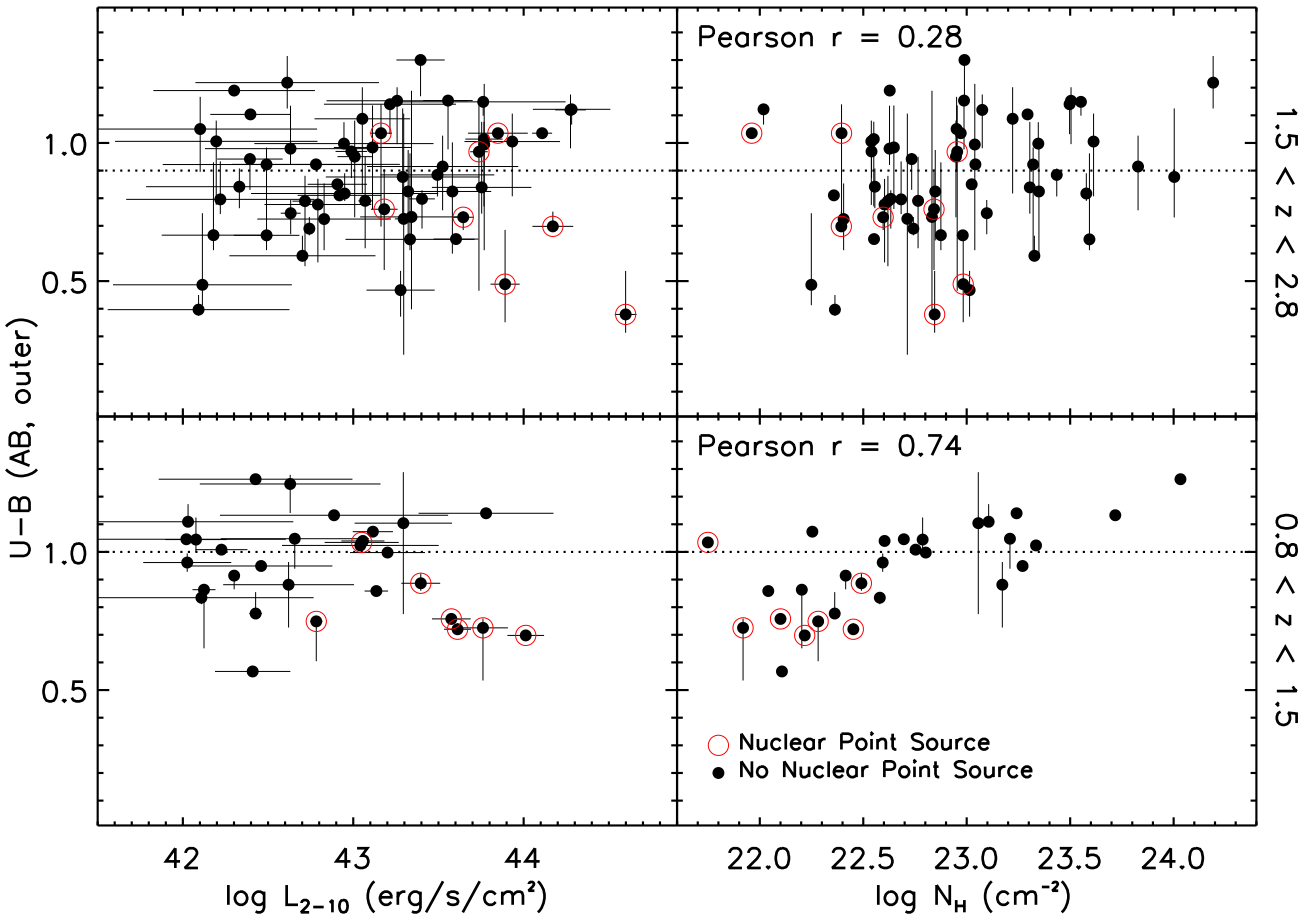

FIG. 9.— The rest-frame outer U-B colors of AGN hosts plotted against hard-band X-ray luminosity $L_{2\text{-}10}$ (left panels) and the Hydrogen column density of X-ray obscuring gas (right panels). The lower panels show AGNs at intermediate redshifts ($0.8 < z < 1.5$), while the upper panels show AGNs at high redshifts ($1.5 < z < 2.8$). A horizontal dotted lines shows the approximate location of the green valley in the appropriate redshift bin. AGNs with strong nuclear contamination, identified based on X-ray criteria, are plotted as concentric circle points.

light spilling into the extended light aperture. As the figure demonstrates, our X-ray based exclusion does an excellent job at flagging these cases.

Among AGNs in the lower redshift interval ($0.8 < z < 1.5$ – lower two panels), a positive correlation may be discerned between the galaxy color and X-ray obscuration. The Pearson coefficient between outer U-B and N_H for uncontaminated AGN hosts is $r = 0.74$, indicating a reasonably strong correlation. This relationship is not due to the exclusion of the luminous X-ray sources, since even the less luminous sources also have blue colors and relatively soft X-ray spectra, while the two galaxies with the hardest spectra are among the reddest in the sample.

Despite a clear trend between obscuration and galaxy color, a clear relationship is not seen between AGN luminosity and galaxy color. There is slight hint that the range of galaxy colors among lower luminosity AGNs ($L_{2\text{-}10} \lesssim 10^{43}$ erg s^{-1}) is larger than among more luminous AGNs, but this is not particularly significant and may be driven mostly by the tail of lower stellar mass AGN hosts, which are generally less luminous than the bulk of AGNs (Fig. 4).

At higher redshifts (upper panels), the trend between X-ray obscuration and host color is much weaker (Pearson $r = 0.28$), and, despite the larger dynamic range in X-ray luminosity probed by our sample, no hint of any relationship between galaxy color and $L_{2\text{-}10}$.

At first glance, the trend between outer U-B and N_H among lower redshift AGNs would suggest that nuclear contamination is still an issue for the extended light photometry, since the soft X-ray sources with more prominent blue nuclear emission at the same X-ray luminosity would scatter more light into the our working annulus. We test this possibility in two ways. First we visually examined the images of the soft and hard sources in this redshift bin for the presence of point sources. None were seen, though the soft sources did show more prominent extended blue light consistent with more star-formation. Secondly, for AGNs in the lower redshift bin where surface brightness dimming is not a major factor, we plotted the U-B color of a larger annular aperture ($0\farcs8 < R_{eff} < 1\farcs6$) against N_H. The larger annulus, coupled with the larger sizes and higher surface brightnesses of the lower redshift galaxies, should weaken any trends arising from the leakage of nuclear light into the outer annular photometry. The trend still remains; indeed, the

color difference between soft and hard X-ray sources becomes more pronounced. This suggests that the relationship between outer color and X-ray obscuration is real, i.e, AGNs with larger levels of extended star-formation host softer, less obscured X-ray sources. A similar result was uncovered for X-ray selected AGNs at the same redshifts by (**?**). At higher redshift, this trends appears to weaken or disappear.

7.3. *Context: Field Galaxy Color-Mass Diagrams*

Before a detailed study of AGN colors, we set the context by examining the properties of inactive galaxies through the use of U-B color-mass diagrams (CMD_*). In the upper three panels of Fig. 10, we plot the CMD_* of galaxies in the three redshift intervals defined earlier: low ($0.8 < z < 1.2$), intermediate ($1.2 < z < 2.0$) and high ($2.0 < z < 2.8$) bins. Galaxies in the general control sample (see §3.2) are plotted as small points and their U-B colors are derived purely from extended light photometry. Using these diagrams, we are able to ascertain the general properties of the field galaxy sample in extended galaxy light, which are likely to differ from those derived from integrated photomety.

We begin by highlighting the bimodality evident in the outer colors of the non-active control galaxies at all redshifts. A Red Sequence from evolved or reddened galaxies can be easily distinguished in the low and intermediate bin panels. A slope to the sequence is discernible, though the data are not sufficient to identify any evolution in the slope. In the high bin, the low-mass end (log $M_* < 10.5$) of the Red Sequence is diminished, but red galaxies can still be found at high masses.

In addition to the Red Sequence, a cloud of blue, star-forming galaxies is also seen, typically at lower masses than the red galaxies. The density of the Blue Cloud in the CMD_*, relative to the Red Sequence, increases with redshift. This is due to a combination of factors. The mean star-formation rate of field galaxies in the early Universe is higher (Noeske et al. 2007), implying a larger space density of star-forming systems. In addition, the FIREWORKS catalog is K_S-band, which corresponds to bluer rest-frame wavelengths at $z \sim 2.5$ compared to $z \sim 1$. Thus, at higher redshifts, a selection based on K_S-band magnitudes is expected to have a relatively larger number of bright blue galaxies than at lower redshifts. Lower mean metallicities in the high redshift systems may also contribute. Since we deal primarily with AGN host properties in this paper, we refrain from a detailed treatment of the form of the bimodality and its evolution with redshift, noting only that a bimodality exists and is well-defined.

The typical color of the Blue Cloud changes with redshift: median U-B values for low/intermediate/high bins are 0.7/0.6/0.45 mag. Again, multiple factors can contribute to this. As the age of the Universe decreases, the characteristic stellar age of star-forming galaxies drops, implying bluer colors. The greater level of star-formation in high redshift galaxies will also contribute to bluer colors.

A third, more subtle reason comes from a combination of the size evolution of galaxies and the red-to-blue radial color gradients of normal star-forming galaxies at these redshifts (e.g. Guo et al. 2011). In the low bin, our annular aperture typically corresponds to a smaller scale than in the higher redshift bins, in terms of galaxy size or half-light radius. Therefore, with redshift, we progressively probe regions that are further out – and therefore, bluer – in a typical galaxy. This leads to an apparent evolution in the median outer color of the Blue Cloud. Indeed, the outer U-B color of blue galaxies from the general control sample are redder than their integrated rest-frame color (from FIREWORKS) by ~ 0.15 mag in the low bin, while they are identical (with large scatter) in the high bin. The Red Sequence shows very little difference between outer and integrated color, which is expected, since most evolved galaxies exhibit flat color gradients.

Finally, we use these CMD_* to evaluate the location of the Green Valley in extended light. We define this to be a dividing line between the Red Sequence and Blue Cloud, corresponding to the region of minimum density in the CMD_* between these two populations of galaxies. Since the Red Sequence has a definite slope with stellar mass, the Green Valley line will also be sloped. For the reasons listed above, we expect the location of the Green Valley to differ slightly from definitions based on integrated photometry (e.g. Willmer et al. 2006); hence we define our own Green Valley lines for our purposes. The low density of points in some of the upper panels of Fig.10, especially on the Red Sequence, prevents sufficient constraints to be placed on the evolution of the slope of the Green Valley across stellar mass. Therefore, we assume that the dividing line that runs through the Green Valley in our U-B CMD_* has a constant slope in all three redshift bins. We calibrate the slope and intercept of the line in the intermediate bin, which has the largest density of galaxies, by varying the line parameters such that the distribution of U-B offsets from the line has a minimum at the location of the line. We derive a slope to the Green Valley line of 0.09 mag per decade in M_*. For the other two redshift bins, we kept the slope constant at this value, but vary the intercept. While a definite Green Valley can be identified in the high bin, a clear minima in the U-B color offsets is not visible in the low bin. In the latter case, we place the Green Valley at the approximate location of a shoulder in the distribution of U-B offsets from the line. The Green Valley lines are shown in Fig.10 with solid green lines.

7.4. *AGN Hosts vs. Inactive Field Galaxies*

The upper panels set the context of the field galaxy population within which we couch the CMD_* of the AGN hosts. In the lower three panels of Fig.10, we again plot the general control sample as small black points, along with the AGNs as red stars and mass-matched control galaxies as black squares. As before, the U-B colors for these galaxies come purely from SED fits to extended light photometry.

Concentrate first on the properties of the AGNs. They occupy a somewhat different distribution in the CMD_* compared to the general control sample at all redshifts. Their stellar masses that are typically higher and their colors that are typically redder. Also, the AGNs have a flatter distribution of colors in this diagram with a weaker bimodality. This tendency has been observed in many previous studies which looked at the integrated photometry of AGNs. We show here that the effect is not due to low levels of nuclear blue light pushing red

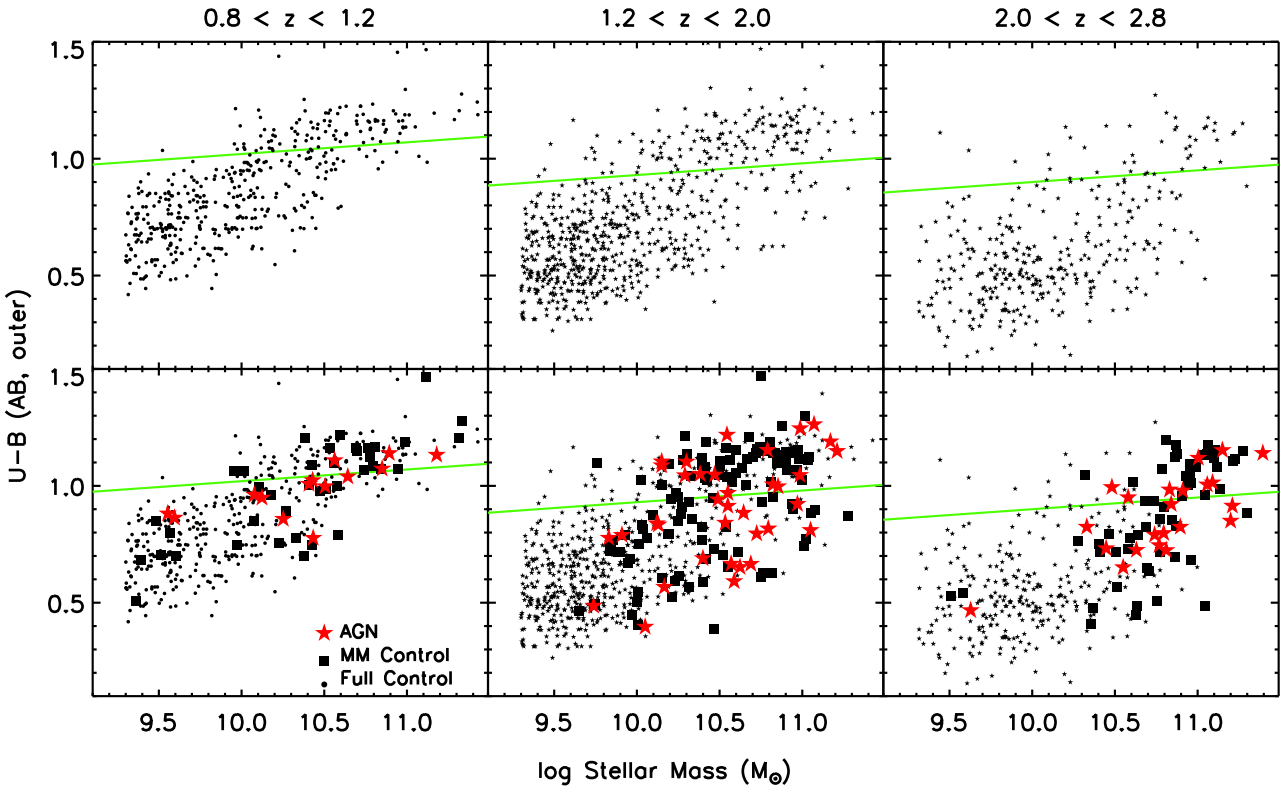

FIG. 10.— U-B color vs. Stellar mass for AGNs and normal galaxies in three redshift bins. The small points are for all galaxies in the FIREWORKS catalog and their colors come from fits to integrated photometry. The large points show extended photometry for AGNs (red points) and magnitude-matched control galaxies (black points). The AGNs tend to have high stellar masses and red colors, while magnitude-matched control galaxies show a larger spread to low masses and bluer colors.

hosts into the Green Valley, but is intrinsic to the stellar populations of the AGN hosts.

A clearer picture of the differences between AGNs and field galaxies sample comes from considering their distribution of U-B offsets. The offset is defined as the difference in the outer U-B color of a galaxy from the Green Valley color at its stellar mass, i.e, it is the offset of the galaxy from the best-choice Green Valley line defined above. We refer to this offset as ΔU-B.

In the left three panels of Fig.11, we compare the ΔU-B distributions of AGNs (solid histograms) and the general control sample (solid histograms) in all three redshift bins. These histograms show the best-fit colors determined from the SEDs and have not been 'regularized' by the bootstrapping procedure described in §5.2. Nevertheless, the difference between the distributions is clear. The general control sample shows a wide range in ΔU-B, with a peak at a negative (blue) value that decreases with redshift. The AGNs, on the other hand, display a narrower distribution that peaks at significantly redder colors, more or less around the Green Valley (ΔU-B= 0). The distribution of AGN colors is narrowest in the low bin and gets progressively broader in the two higher redshift bins. Note that this broadening is unlikely to be due to a larger errors in the photometry of higher redshift galaxies. The median errors in the ΔU-B of the AGNs are shown above the histograms and are generally much smaller than the widths of the color offset distibutions.

We compare the distributions of the control sample and AGNs using a Kolmogorov-Smirnov (KS) test, which gives us the probability P_{KS} that the two distributions are as different as we observe them to be despite being actually identical. P_{KS} for the general control sample are all less than 1%, i.e, the differences in the distributions are significant are better than 99% in all three bins.

7.5. *Stellar Mass Selection Effects*

Returning now to Fig.10, we examine the location of the mass-matched control sample in the CMD_*(black squares). Unlike the general control sample, the galaxies of the mass-matched control sample lie in a similar part of the diagram as the AGNs. In particular, they share their flatter color distribution and high masses. The fact that the AGN and mass-matched control galaxies have similar masses is, of course, simply a construction of the mass-matching method.

We are in a position now to tease apart stellar mass selection effects from factors related to SMBH accretion among X-ray selected AGNs. The right set of panels in Fig.11 compares ΔU-B distributions of the AGNs (filled histograms) and the mass-matched control sample (open histograms) in the three redshift bins. A simple comparison of the middle and right panels shows that the mass-matched control sample is a much better match to the color distribution of the AGNs than the general control sample. In particular, the range in ΔU-B and the peak value of the mass-matched histograms are now quite similar to the AGNs. P_{KS} for the mass-matched control sample compared vary from 36% in the low bin to 85% in the intermediate bin, much higher than for the general control sample.

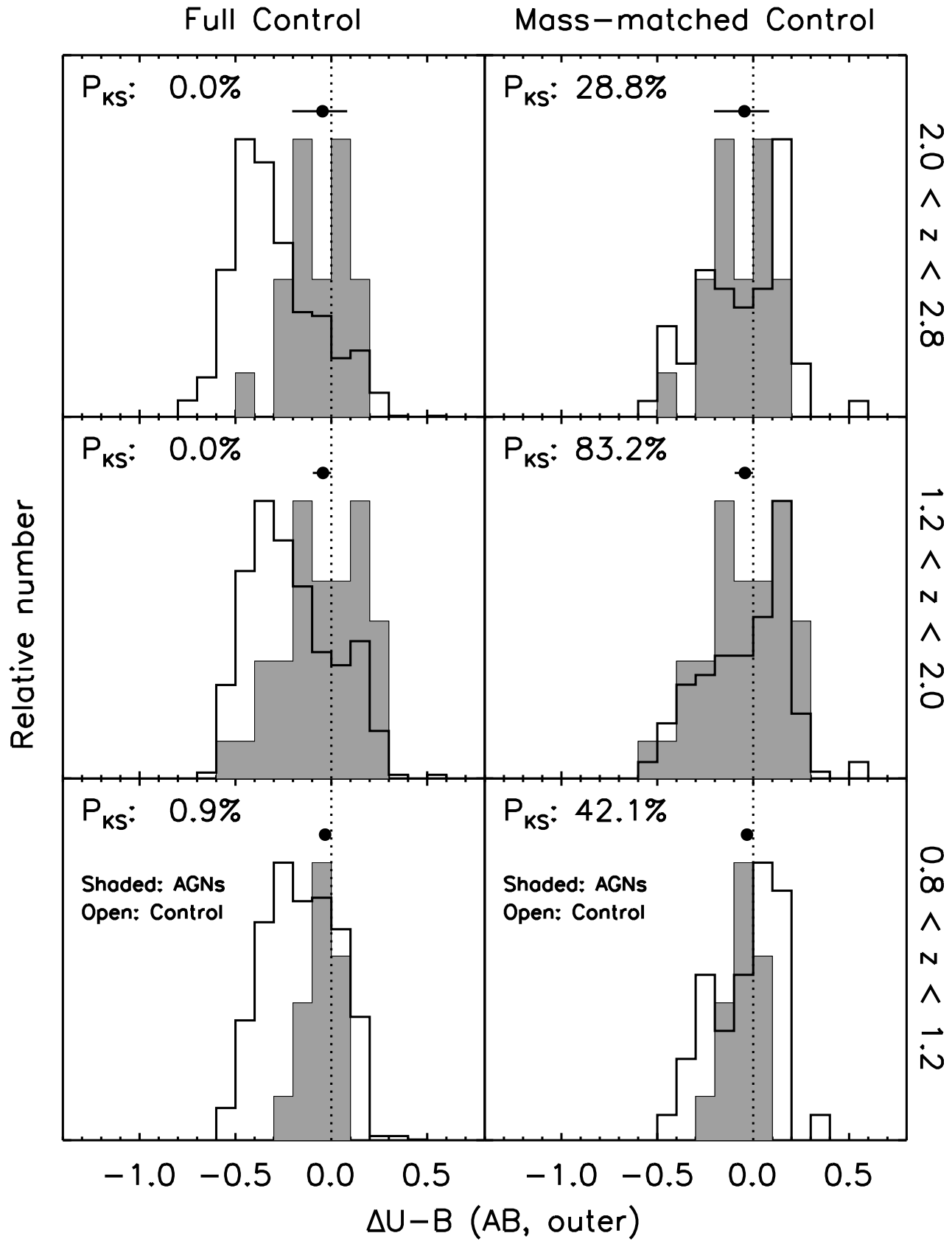

FIG. 11.— Rest-frame U-B color distributions of the extended light in an annular aperture of radial size from $0\farcs4 - 1\farcs0$ in three redshift bins, increasing in median redshift from bottom to top. The left panels show the U-B distribution with respect to the general control sample, while the right panels are a comparison to the mass-matched control sample. The Kolmogorov-Smirnov probability P_{KS} is a measure of the likelihood that the two distributions are derived from the same parent distribution.

Simply matching in stellar mass leads to a distribution of U-B colors among inactive galaxies that is much more similar to that of the AGN hosts. This is because X-ray detected AGNs are much more likely to be found in massive galaxies than low mass galaxies. These massive hosts tend to be redder and have lower levels of star formation than the general population of field galaxies. Recall that the general control sample were selected to have the same range of stellar mass and optical luminosity as the AGNs, but were not restricted to have the same *distribution* in mass as the AGNs. Even choosing a control sample to have the same range of mass as the AGNs is not sufficient to correct for stellar mass selection effects. Careful mass-matching is critical.

We may conclude from this exercise that stellar mass selection effects are the primary cause of any differences in the color distributions of active and inactive galaxies. This is consistent with the results from the study of Xue et al. (2010) using the CDF-S 2MSec survey.

7.6. *AGN Hosts vs. Galaxies of similar M_**

We now turn to a closer examination of the U-B colors of AGN hosts and mass-matched inactive galaxies. The right panels of Fig.11 show similarities in the colors, but some systematic differences in the histograms remain. The differences are most pronounced in the low bin, where the ΔU-B distribution of the AGNs appears to be significantly narrower than the control sample, at a significance level of $1-P_{KS} \sim 60\%$. However, stochastic effects from the small size of the AGN sample and the large uncertainties in the colors of some galaxies can complicate our interpretation of these differences.

To account for stochastic effects more accurately, we 'regularize' the ΔU-B distributions of the AGNs and mass-matched control sample using the monte-carlo bootstrapping procedure (§5.2). The results are shown in Fig. 12. The left panels of the figure plots the regularized distributions of ΔU-B for AGNs (solid histograms) and mass-matched inactive galaxies (open histograms) in the same three redshift bins. Error bars on the open histograms give the 1σ uncertainty on the distribution of the control sample. As discussed in §5.2, these errors take into account the stochasticity of the small AGN sample size as well as modeling errors. In each of these panels, we also show P_{KS} determined from the unregularized distributions, in order to provide a sense of how they differ before the application of the bootstrapping process.

We concentrate first on a comparison of AGN host color distributions across redshift. In the low bin, one finds a fairly tight range in ΔU-B, spanning about 0.6 mag and peaking sharply at the Green Valley (ΔU-B= 0). In the intermediate and high bins, the peak offset still remains roughly fixed. However, the width of the distribution changes considerably between the higher redshift bins and the low bin, with a larger scatter towards red and blue colors. The largest increase is in the fraction of galaxies with blue U-B colors (negative ΔU-B). Since we have conservatively removed all cases where blue nuclear light could potentially contaminate extended light in the AGN hosts, this evolution in color could be a consequence of younger light-weighted mean ages in high redshift AGN compared to low redshift AGN, or an evolution in the mean metallicity or dust obscuration with redshift. A very similar evolution in the U-B color distribution is also evident in the mass-matched control sample. This again underlines the fact that this color evolution is not due to any increasing contribution from AGN light, as this would not be manifested among inactive galaxies. Since the fraction of actively star-forming galaxies is known to increase considerably between $z \sim 1$ and $z \sim 2$ (for e.g, Fig. 10), the bluer colors at high redshifts in both AGNs and inactive galaxies is likely to be primarily due to an evolution in mean ages of the stellar populations in these galaxies. We confirm this later in our examination of SFHs (§9).

Comparing now the color distributions of AGN hosts and control galaxies in the left panels of Fig. 12, we see that, by and large, the histograms are quite similar in the all the redshift bins, as was the case for the unregularized distributions. However, the control sample still tends to show a more pronounced bimodality than the AGNs. In other words, the color distributions of the AGNs tends to be flatter than that of inactive galaxies, even after mass-matching.

The largest significant differences are observed in the low bins. Here, the ΔU-B distribution of the mass-matched control spreads to redder and bluer colors, while the AGNs show a tighter distribution, peaking in the Green Valley. In the intermediate bin, the two distributions have almost identical widths and wings, but there exists a small and marginally significant difference in the modal color of the AGNs compared to the control with an offset to bluer colors of about 0.15 mag. A similar situation holds in the high bin, though the control sample also exhibits a slight excess of blue galaxies.

While the general consistency between the colors of AGNs and inactive galaxies of the same stellar mass implies that their stellar populations are also quite similar, certainly when compared to the general field population, one may wonder if other effects could influence this interpretation. For example, could differences in the level of dust obscuration in AGN hosts hide possible differences in stellar populations, or be responsible for the small differences we observe between the modal colors of AGN hosts and inactive galaxies? For example, Cardamone et al. (2010) find that the application of a dust obscuration correction to the colors of AGN hosts at $z \approx 1$ leads to a pronounced bimodality, paralleling the properties of normal Green Valley galaxies. To explore possible effects from dust obscuration, we plot, in the right panels of Fig. 12, distributions of the intrinsic ΔU-B for the AGN hosts and mass-matched control galaxies. This is difference between the unextincted rest-frame U-B color of the best-fit stellar synthesis model and that of the Green Valley at the mass of the galaxy. In essence, these are the rest-frame U-B offsets of the the galaxies, after de-reddening by an amount corresponding to the extinction from the SED-fits.

Comparing intrinsic and measured color distributions (right and left panels respectively), one sees that the dust obscuration acts to move some galaxies with very blue intrinsic colors (young mean ages) towards the red, tightening the overall color distribution of galaxies. In the right panels, the color distributions of both AGNs and inactive galaxies are now much broader, with a much more pronounced and bluer cloud of star-forming galaxies, especially among the inactive sample. However, the trends that appear in the left panels are also repeated in

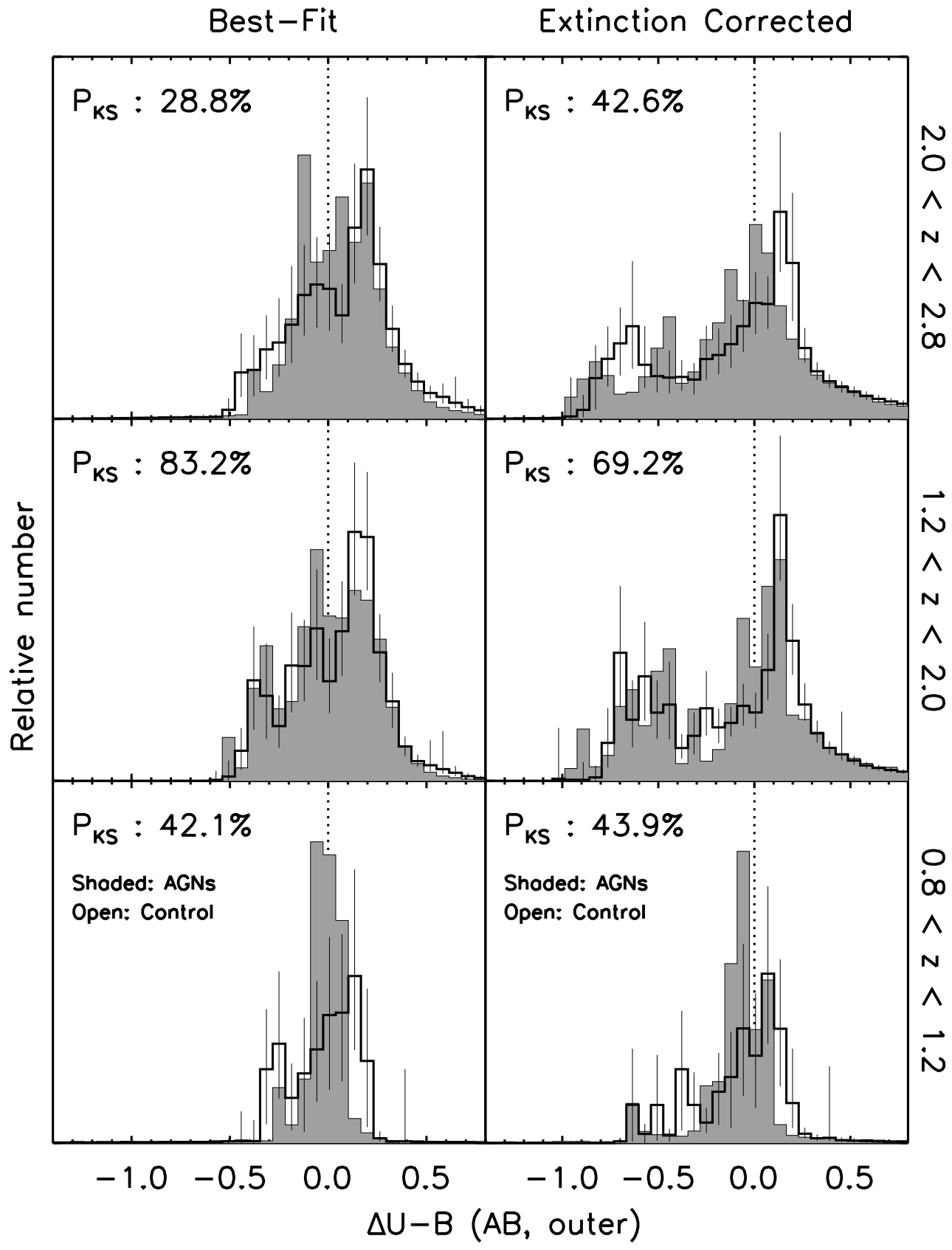

FIG. 12.— Rest-frame U-B color distributions of the extended light in an annular aperture of radial size from $0\farcs4 - 1\farcs0$ in three redshift bins, increasing in median redshift from bottom to top. The left three panels on the left show the distributions of best-fit color, while the panels on the right show the distributions of color for best-fit SED models before applying any extinction (in essence, an extinction-corrected color of the galaxy). These distributions have been regularized by a monte-carlo bootstrap procedure (§5.2).

the right panels. The significant tendency for AGN colors in the low bin to peak in the Green Valley remains, at odds with the results of Cardamone et al. (2010). In the intermediate and high bins, the AGNs and control galaxies show rather similar distributions, with a small, barely significant tendency to peak at colors that are ~ 0.1 mag bluer than the peak of the mass-matched control galaxies, placing them marginally closer to the Green Valley.

Before embarking on an interpretation of these color differences, we explore the degree to which such differences arise simply from the limitations of the mass-matching process. The CMD_* in the top panels of Fig. 10 indicates that fraction of blue galaxies increases greatly among the field galaxy population towards higher redshifts. Since we have allowed the mass-matched control sample to include galaxies that can be as much as a factor of two less massive than the AGN hosts, a larger fraction of lower-mass blue galaxies will make it into the control set towards progressively higher redshifts, just due to greater errors in the stellar masses and the much greater density of blue galaxies. For these reasons, a general trend towards increasing numbers of blue galaxies among the inactive sample compared to AGNs may be expected from the finite tolerances of the mass-matching procedure. Therefore, the second order changes that we see between AGN and control galaxies in the high redshift bins, especially with regards to the blue tail of the distribution, should be considered tentative.

However, scatter due to stellar mass errors will not substantially affect galaxies in the low bin, which are brighter at all bands, have better photometry and better sampled SEDs. The significant preference for AGNs to lie in the Green Valley, even after accounting for galaxy extinction, implies that there is a close relationship between AGN activity and galaxy color at $z \sim 1$. AGN hosts at these redshifts do indeed prefer to lie in galaxies with intermediate levels of star-formation activity.

To summarize: At all redshifts, hosts of AGN tend to have redder colors and a flatter color distribution than the general field population of galaxies (bottom panels in Fig. 10) This is consistent with results from many previous studies: AGN tend to be in hosts that lie on the Red Sequence or 'Green valley' (Kauffmann et al. 2003; Nandra et al. 2007; Brusa et al. 2009; Schawinski et al. 2010; Xue et al. 2010; Cardamone et al. 2010). However, restricting the comparison to the mass-matched control sample, the differences between AGN hosts and non-active galaxies reduces significantly. At $1.2 < z < 2.0$, where we have the largest number of galaxies in both samples, the color distributions of the two populations are very similar ($\mathrm{P_{KS}} \sim 80\%$). This similarity in colors between AGN and non-active galaxies of the same mass at these redshifts is consistent with other studies of integrated and resolved stellar populations in AGN (Xue et al. 2010; Ammons et al. 2011). The modal colors of AGN hosts are a bit bluer than the modal color of the mass-matched control galaxies, by around 0.1–0.2 magnitudes, which suggests a slight, though not very significant, inclination of AGN hosts towards intermediate colors.

The largest and most significant differences in color are found in the low bin, at $z \approx 1$. The AGNs at this epoch show a preference for lying in the Green Valley at the expense of being under-represented in the Red Sequence or Blue Cloud, even when the effects of dust reddening are corrected. In our highest redshift bin, at $2.0 < z < 2.5$, the mass-matched control sample includes significantly more blue galaxies compared to AGNs. We suggest that this comes primarily from the more uncertain stellar masses coupled with the strong evolution in the number density and colors of the star-forming galaxy population towards these redshifts.

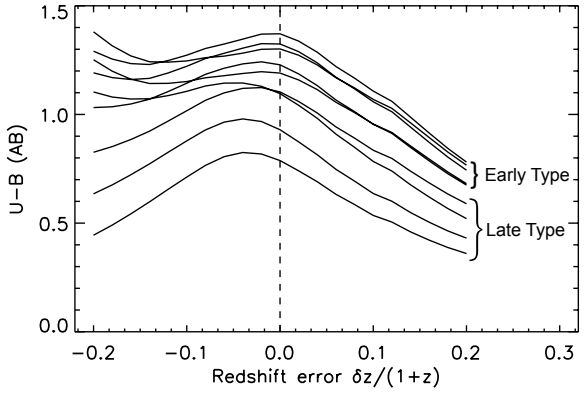

FIG. 13.— The effects of redshift errors on the U-B colors of galaxies. Each line tracks the color of a certain spectral template of a model galaxy as the redshift error δz is increased or decreased by upto 20% of $1+z$. Due to the sharpness of the Balmer/4000Å break, redshift errors tend to lead to bluer colors, irrespective of the sign of the error. The characteristic redshift error of galaxies in this study is $|\delta z/(1+z)| = 0.07$.

7.7. *Effect of Redshift Errors*

The U-B color is sensitive to the strength of the 4000 Å break, and hence to the light-weighted mean age of the stellar population of a galaxy. However, in real galaxy catalogs with redshift errors, the error in the color can depend in a complex manner on the redshift errors of the galaxy. This is because galaxy spectra frequently display prominent Balmer or 4000 Å breaks. If the true redshift of a galaxy is different from the redshift used in the derivation of the rest-frame U-B color due to an error in the cataloged redshift, the synthetic photometry from our SED fits will span wavelengths blue-ward or red-ward of the break, where the slope of the galaxy light tends to be shallower than across the actual break. Hence, redshift errors tend to lead to bluer U-B colors irrespective of the sign of the error. In other words, the synthesized U-B color distribution for a range of galaxy SED templates, such as our τ-model library, in the presence of a range of redshift errors, will be biased bluer the true U-B color distribution of the templates without redshift errors.

This is potentially important since a large number of our high redshift AGN and more than 50% of the control galaxy sample do not have highly accurate spectroscopic redshifts, but instead have photometric redshifts with considerable uncertainty. The characteristic absolute value of $\delta z/(1+z)$ for galaxies with photometric redshifts in the mass-matched control sample is 0.07, and around 90% have an estimated $|\delta z/(1+z)| < 0.1$ Hence, one may expect that model U-B colors for the objects with photometric redshifts would be preferentially bluer, which may affect our comparison of the colors of these galaxies.

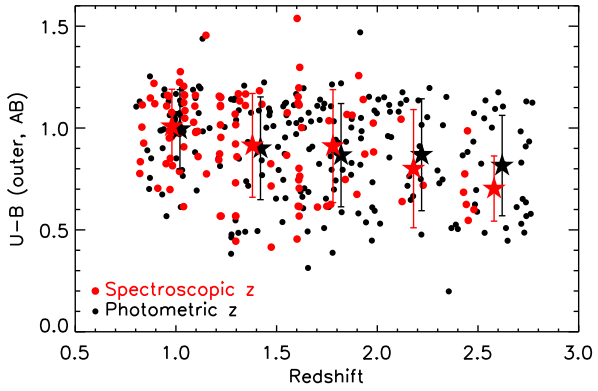

FIG. 14.— Rest-frame outer U-B color vs. redshift of inactive galaxies from the mass-matched control sample. The black points are galaxies with purely photometric redshifts, while the red points are galaxies with spectroscopic redshifts. The red and black points have very similar color distributions, which implies that the effect of photometric redshift errors on the color distributions of the control sample (see Fig. 12) are small to negligible. The mean color in five redshift bins are shown as large star-shaped points. Beyond a redshift of 2, the objects with spectroscopic redshifts tend to have slightly bluer colors than objects with photometric redshifts, presumably because of selection effects that favor blue star-forming galaxies with emission lines or strong Lyman breaks in such high redshift spectroscopic samples.

The degree of this effect is shown in Fig.13, in which we have plotted simulated U-B colors for a set of representative galaxy spectral templates from the SWIRE template library (Polletta et al. 2007); three quiescent galaxy templates with ages between 2-13 Gyr ('Ellipticals') and six star-forming galaxies with varying degrees of current star-formation ('Spirals'). The galaxy templates were shifted in wavelength to simulate the effects of a redshift error δz, parametrized in the figure by the $\delta z/(1+z)$. The simulated colors are reddest at δz between -0.02 and 0.0, depending on the template, but get progressively bluer as the redshift errors get both larger or smaller. Due to the sharpness of the Balmer/4000Å break, redshift errors tend to lead to bluer colors, irrespective of the sign of the error.

We constrain the importance of this effect on our rest-frame colors by comparing the U-B distributions of the mass-matched control galaxies with and without spectroscopic redshifts. In Fig. 14, we plot the U-B colors of these two sets of control galaxies against redshift. The distribution of the black points (galaxies with photometric redshifts) is very similar to those of the red points (galaxies with spectroscopic redshifts) and clearly do not appear to be systematically bluer. In fact, at the highest redshifts ($z \sim 2.5$), the objects with spectroscopic redshifts tend to be a little bluer, probably because bright FUV continua or strong line-emission, both associated with blue star-forming galaxies, are necessary to find good spectroscopic redshifts for such distant galaxies.

From this we can conclude that photometric redshift errors for the control sample do not introduce strong systematics in the U-B color distributions of the galaxies. A likely cause for the weakening of this effect is that galaxies with prominent spectral features, such as breaks, usually have better determined photometric redshifts as a consequence of the sharpness of the break, which works against the severity of the effect. The trends in Fig. 12 are likely to reflect the true colors of the AGN and control galaxies.

8. COLOR GRADIENTS

Radial gradients in color are sensitive to the inside-out distribution of star-formation across a galaxy. Coherent trends in the color gradients of galaxies measure the direction in which a normal galaxy builds its stellar mass through star-formation, and serve as tracers of the relative star-formation history across a galaxy.

Color gradients are an important constraint on the role of nuclear activity in the regulation of star-formation in AGN hosts. If AGN are directly responsible for the shut down of star-formation in massive galaxies, a difference is expected in the gradients of AGNs and inactive galaxies of a similar stellar mass. The time-scale over which feedback from an AGN blows out a galaxy's gas will determine the steepness of the gradient. The luminosity of the AGN is likely to regulate the scale over which the gradient may be measured - low luminosity AGN only supply enough energy and radiation pressure feedback to influence the very inner parts of a galaxy.

In §7.5, we show that the outer colors of AGN hosts are consistent with those of normal galaxies of the same mass. This suggests that the outer stellar populations of AGN hosts are the same as inactive galaxies and the suppression of star-formation by feedback effects does not extend beyond a few kpc, at least for AGNs in the luminosity range probed ($L_{2\text{-}10} \lesssim 45$ erg s^{-1}). How do the nuclear colors of AGN hosts, relative to the outer colors, compare to those of inactive galaxies?

In Fig. 15, we compare the gradients in the rest-frame U-B colors of the AGNs (large colored star points) and mass-matched control sample (small black points) against their outer U-B colors, in two redshift bins. Gradients are calculated as the difference between the outer and nuclear U-B colors, i.e, colors from fixed apertures of radius 0.″4-1.″0 (annular) and 0.″1 respectively. A lower/higher value of the gradient implies a bluer/redder outer color, with the dotted line showing a flat gradient. In addition, we use colors for the star points to indicate the X-ray luminosity of the AGNs, from $L_{2\text{-}10} = 10^{42}$ (black stars) to $L_{2\text{-}10} = 10^{44.5}$ (red stars). The AGNs with nuclear contamination are included in the figure as large concentric star points.

A key first observation is that the median gradient of both uncontaminated AGNs and control galaxies is negative, with most points lying below the flat-gradient dotted line. Therefore, both AGNs and inactive galaxies are generally redder in the central few kpc, compared to their outskirts. The median offset from a flat gradient varies from ≈ -0.16 in Bin A to ≈ -0.25 in Bin C. The scatter in the gradient also increases considerably towards high redshifts. The source of this change in the median and the scatter could be intrinsic to the galaxy population, but it is also influenced by the accuracy of PSF matching (to which the nuclear colors are particularly sensitive) as well as the larger errors in photometry suffered by the more distant galaxies. This is why a careful control sample processed through the same selection criterion, photometric measurement and modeling method is critical to constrain true differences in the color gradients between AGNs and normal galaxies.

In general, the form and scatter of the distribution

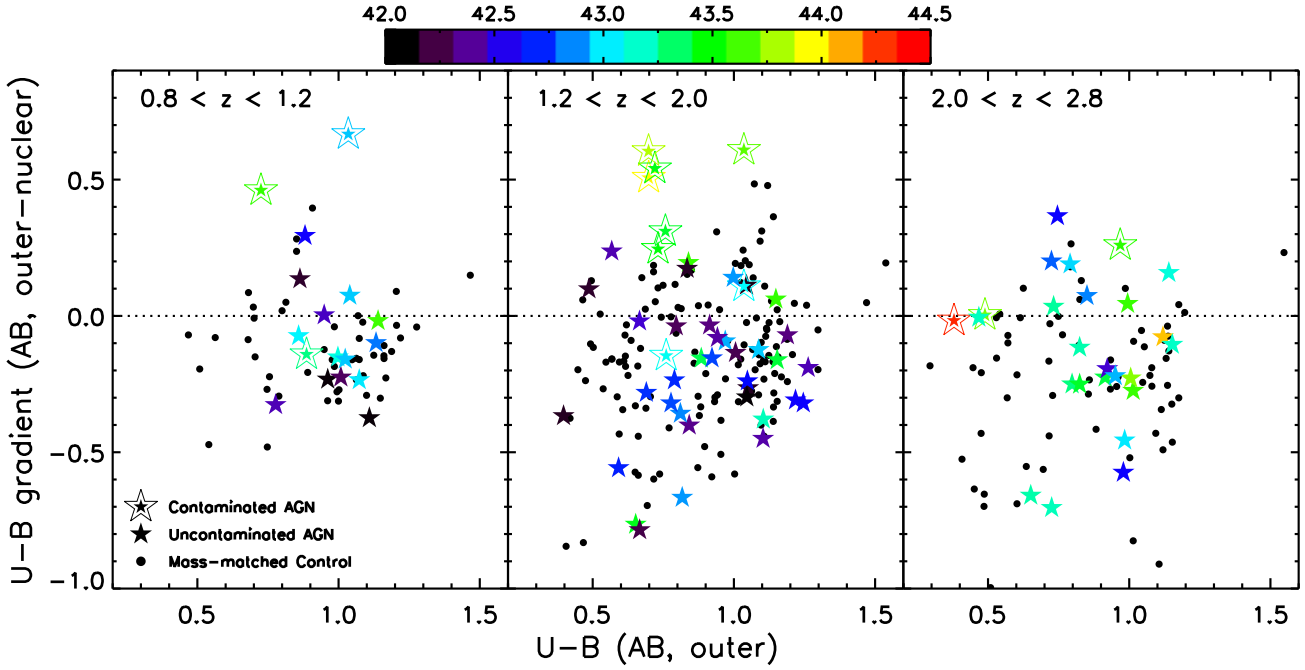

FIG. 15.— Rest-frame U-B color gradients (outer - nuclear) plotted against the outer U-B color, in three redshift bins. AGNs are shown by colored star points, where the color represents the hard band X-ray luminosity $L_{2\text{-}10}$ (as shown by the color bar). The small black points are the mass-matched control sample of inactive galaxies.

of color gradients between uncontaminated AGNs and inactive galaxies are similar, implying that, by-and-large,

Close examination of the colored points relative to the black points reveals an interesting trend. The luminous AGNs in Fig. 15 (cyan to red points) tend to lie closer to the dotted line compared to the the lower luminosity AGNs (black to blue points), implying that they have a flatter color gradient. We explore this further in Fig. 16, where we have plotted the color gradient against the X-ray luminosity in two redshift intervals: $0.8 < z < 1.5$ and $1.5 < z < 2.8$.

In the left panel, a weak positive correlation is present, but the limited dynamic range in X-ray luminosity among AGNs in this redshift bin prevents the discernment of a clear trend. In the right panel, the picture is somewhat clearer. There is a scatter of points towards low U-B color gradients (U-B gradient < -0.5) from galaxies that show substantial star-formation in their outskirts. This scatter is seen as well among inactive galaxies in the mass-matched control sample (Fig. 15). If one disregards this scatter, the remaining points show an increase in the U-B gradient towards higher X-ray luminosity. As a guide to the eye, we indicate this trend in the figure by a dashed line derived from a linear regression fit to all data points in the right panel with a gradient > -0.5. The same line, derived from the AGN sample at $1.5 < z < 2.8$, is also shown in the left panel. The linear relationship derived for the high redshift AGNs is consistent with the weak correlation found among the lower redshift AGN.

We have shown in §7.2 and Fig. 9 that the outer colors of AGN hosts show no relationship to the X-ray luminosity of the AGN, especially at $z > 1.5$. Therefore, the correlation between color gradient and $L_{2\text{-}10}$ is due to a change in the nuclear colors of AGNs with X-ray luminosity. More luminous AGNs have bluer nuclear colors, with a substantial scatter (the standard deviation about the mean relation for the AGNs which give the dashed line in Fig. 16 is 0.19 mag).

This behavior of the uncontaminated AGNs may be contrasted with that of the contaminated AGNs (concentric circle points). The typical gradients in these objects are strong and positive (i.e, blue towards the center), consistent with the presence of bright blue point sources. In general, the gradient of the contaminated AGNs are steeper and more positive than uncontaminated AGNs at the same X-ray luminosity, especially in the low redshift sample. This implies that the contaminated and uncontaminated AGNs are not part of a single sequence of galaxies with increasing levels of AGN light in their nuclear aperture, consistent with the idea that contaminated AGNs are optically unobscured, while uncontaminated AGNs show large levels of optical obscuration towards the nuclear source.

Such blue nuclear colors could arise for two possible reasons. There may be a direct link between black hole accretion and the formation of young stars within the inner kpc of the AGN host. Such links have been proposed in studies of local AGNs (e.g. Davies et al. 2007). Or, alternatively, even fairly obscured AGNs may have some fraction of their nuclear emission scattered into the line of sight. The contribution of such scattered AGN emission to light from within the nuclear aperture becomes more important for luminous AGNs, which may explain the trend. At the point, we are unable to distinguish clearly between these two explanations, but further studies of detailed color profiles for luminous AGNs or the analysis of CANDELS grism spectral of AGNs at high angular resolution (e.g., Trump et al. 2011) may help to address this question.

9. STAR-FORMATION HISTORIES OF AGN HOSTS

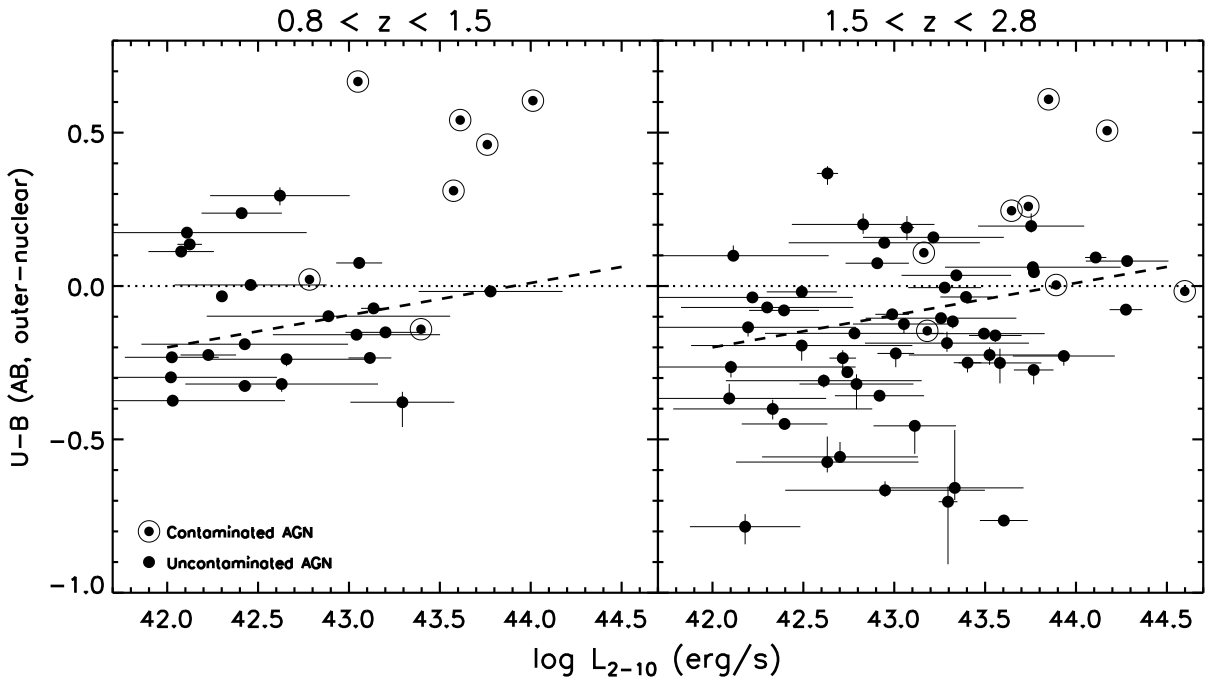

FIG. 16.— Rest-frame U-B color gradients (outer - nuclear) of AGN hosts plotted against hard-band X-ray luminosity, in two redshift intervals. There is a substantial scatter of points towards steep gradients and bluer outer-colors among AGN hosts in the right panel, which is also seen in inactive galaxies at these redshifts (Fig. 15). Despite this scatter, a positive correlation exists between U-B gradient and AGN luminosity.

As we demonstrate in previous sections, the introduction of the high-resolution NIR imaging from WFC3 enables us to sample the rest-frame NUV-optical light of AGN hosts on the scale of the host galaxy, while not being contaminated by nuclear emission in most objects. The detailed sampling of the SED using 6-7 broad photometric bands enables us to fit for the light-weighted star-formation histories (SFHs) of these AGNs, as well as the samples of inactive galaxies, using a suite of increasing and decreasing τ models, as well as constant star-formation rate models (§5). Here we analyze these SFHs and place AGN hosts in the context of field galaxies.

In Fig. 17, we plot, as large red points, the estimated best-fit ages of the AGN host stellar populations against the best-fit exponential time-scales τ. The mass-matched control sample of inactive galaxies is shown using small black points. Models with constant SFHs are also represented in this diagram as points with $\tau = 100Gyr$. Galaxies which are fit with exponentially increasing SFHs are plotted as open circles, while those with exponentially decreasing and constant SFHs are plotted as filled points. The data points have been randomly shifted from the best fit values by a small amount to improve the visibility of points, especially in parts of the diagram with a high density of galaxies. The dashed lines mark the location of models where the population age is equal to τ - among decreasing τ models these are systems in which most of the stellar mass at that redshift has already been formed.

As for the outer U-B colors, AGNs and mass-matched control galaxies show rather similar SFHs. The red and black points occupy the same parts of the age-τ plane and show roughly the same fraction of open and filled points in the diagram.

The dominance of exponentially increasing SFHs among AGNs and similar mass galaxies is clear from the large number of filled points compared to open circles in this diagram. This is consistent with their high stellar masses and relatively red colors, even out to $z \sim 3$. Among AGNs and control galaxies in the low bin ($0.8 < z < 1.2$), essentially none have flat or increasing SFHs. The fraction of galaxies with flatter or constant SFHs increases in the intermediate and high bins(13% at $1.2 < z < 2.0$ and 23% at $2.0 < z < 2.8$), but is still quite low. Most AGNs with $\tau < 0$ lie below and to the right of the dashed line in the figure, implying that their main era of star-formation has now passed. In contrast, galaxies with $\tau > 0$ (open points) on or to the left of the line, indicating that they have formed recently and are currently going through a major phase of star-formation. Such systems, though, are as common among X-ray sources as among inactive galaxies.

The light-weighted stellar age is one of the fundamental physical characteristics of the SFH of galaxies. However, typically the age is quite hard to estimate accurately as it can be degenerate with both the metallicity of the stellar population and the level of dust extinction. Therefore, the confidence intervals on the stellar age from our SED fits can be quite large and are typically skewed towards young ages. In order to make statistically valuable conclusions about the age distributions of the AGNs, and their comparisons with normal galaxies, we apply the monte-carlo bootstrap procedure to arrive at more representative age distributions for the galaxies.

The results are shown in the left panels of Fig. 18. As before, the AGNs are shown as shaded histogram, while the control sample are shown as an open histogram, in the low, intermediate and high redshift bins. In the low bin, the control galaxies show a relatively broad range of ages. The AGNs have a distribution that is a bit narrower than the control sample, but not significantly.

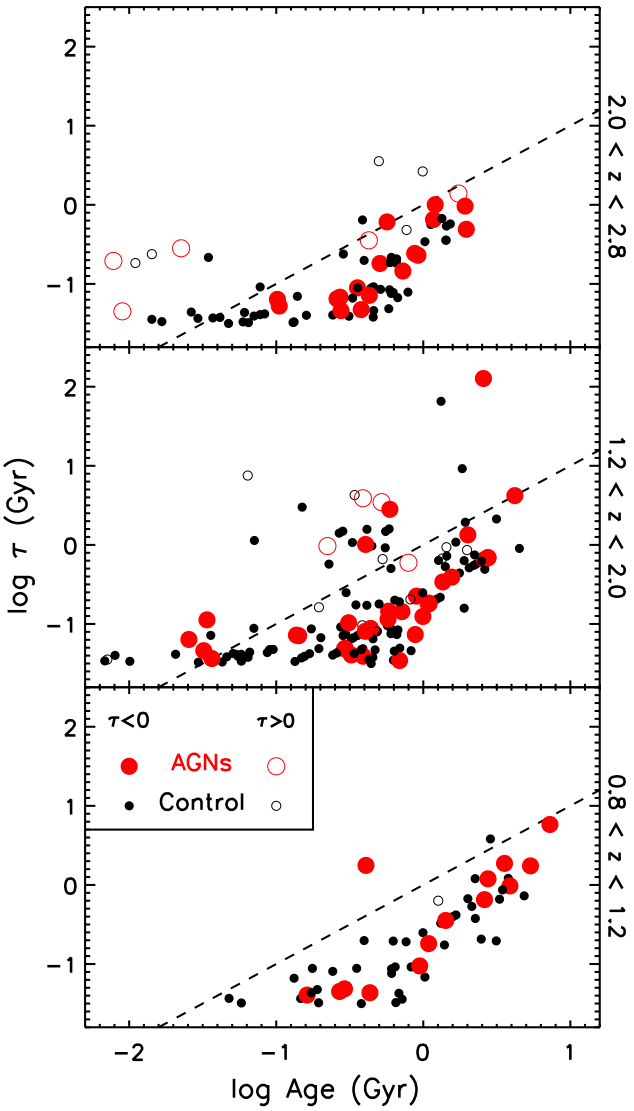

FIG. 17.— Star-formation history (SFH) parameters of AGNs (red points) and mass-matched control galaxies (black points), derived from fits to photometry in an extended annular aperture. τ is the characteristic timescale for exponential SFH histories (constant SFHs are shown in this plot with $\tau = 100$ Gyr). Filled points are galaxies which are best fit by declining exponential SFHs, while open points are galaxies fit with exponentially increasing SFHs. The dashed line corresponds to SFHs where age=τ.

To the uncertainties of the sample, the distributions are very similar.

In the higher redshift bins, the sample sizes of both AGNs (and, by extension, mass-matched control galaxies) are 2 to 3 times larger, making for better defined age histograms. The control galaxies in the intermediate and high bins show a broad but definite peak at 2 Gyr and another smaller narrow peak at ≈ 100 Myr. Compared to the low bin, there is a larger fraction of inactive galaxies with younger ages, stretching down to our lower age limit of 10 Myr. This is consistent with the larger fraction of blue galaxies at higher redshifts among the mass-matched sample as well as the AGN hosts.

The AGNs in the intermediate bin and high bins again appear to be quite similar to the control sample, though in both bins, the AGN distribution is a bit narrower than the control. In addition, in both bins, the AGNs do not show the second peak in the age distribution at young ages which is seen in the control sample. This difference is fairly significant (at the 2σ level), but may be related to the limitations of mass-matching at higher redshifts.

The peak of the distribution in the intermediate bin is slightly offset to younger ages, by a factor ~ 2 compared to inactive galaxies at this redshift, again at a modest level of significance. This difference is not seen at high redshift and the small differences in P_{KS} between the ages in all three bins suggests that the difference in the peaks are probably due to stochastic effects.

We also explore, from our SFHs, the degree to which AGN hosts have built up their stellar content at all these redshifts. We define a parameter called the 'normalized age', which is the ratio of stellar age to τ. This parameter, for declining τ models, indicates how much older a particular galaxy is compared to the timescale over which most of its stars form. In the right panels of Fig. 18, we compare normalized age histograms of AGNs and control galaxies in our three redshift bins. Only objects with declining τ models are used in these histograms, since the normalized age has a different interpretation for exponentially increasing or constant SFH models. We have derived the normalized age and its confidence intervals using the same procedure as any other quantities, i.e, from the full χ^2 space of SED model fits. We also employ the same two-loop monte-carlo bootstrap procedure described above to derive the histograms in the figure.

One may see that at all redshifts considered, the normalized age distributions for AGNs and control galaxies peak at values greater than 1. The distribution is quite narrow at $z \sim 1$, but get progressively broader at higher redshifts as a strong tail develops to very high values. This is because, for these fainter galaxies, τ is very weakly constrained and low τ values lead to progressively higher normalized ages. The tails are an artifact of the regularization process and are not seen in the best-fit distributions.

In the intermediate and high bins, the peaks and widths of the distributions are very similar and the P_{KS} values are reasonably high, indicating that the best-fit distributions are significantly different. Only in the low bin do both P_{KS} drop considerably ($\lesssim 10\%$). The histograms also appear to show some differences at a level of roughly 2σ, where the AGNs display a narrow distribution of normalized ages and a weaker tail to long ages than the control sample. In essence, this means that at $z \approx 1$, the normalized ages of AGNs are slightly shorter and have less variation than inactive galaxies of the same mass.

10. DISCUSSION

10.1. *The Colors and SFHs of AGN Hosts*

WIth the high spatial resolution and unparalleled sensitivity of the WFC3 camera, we have examined the photometric properties and star-formation histories of AGN host galaxies in the CANDELS/CDF-S field at redshifts in the range $0.8 < z < 2.8$. We develop a method, based on X-ray properties, to exclude objects where AGN contamination, scattered from a bright nuclear point source, affects the extended galaxy photometry, revealing, for the first time, the unadulterated extended galaxy stel-

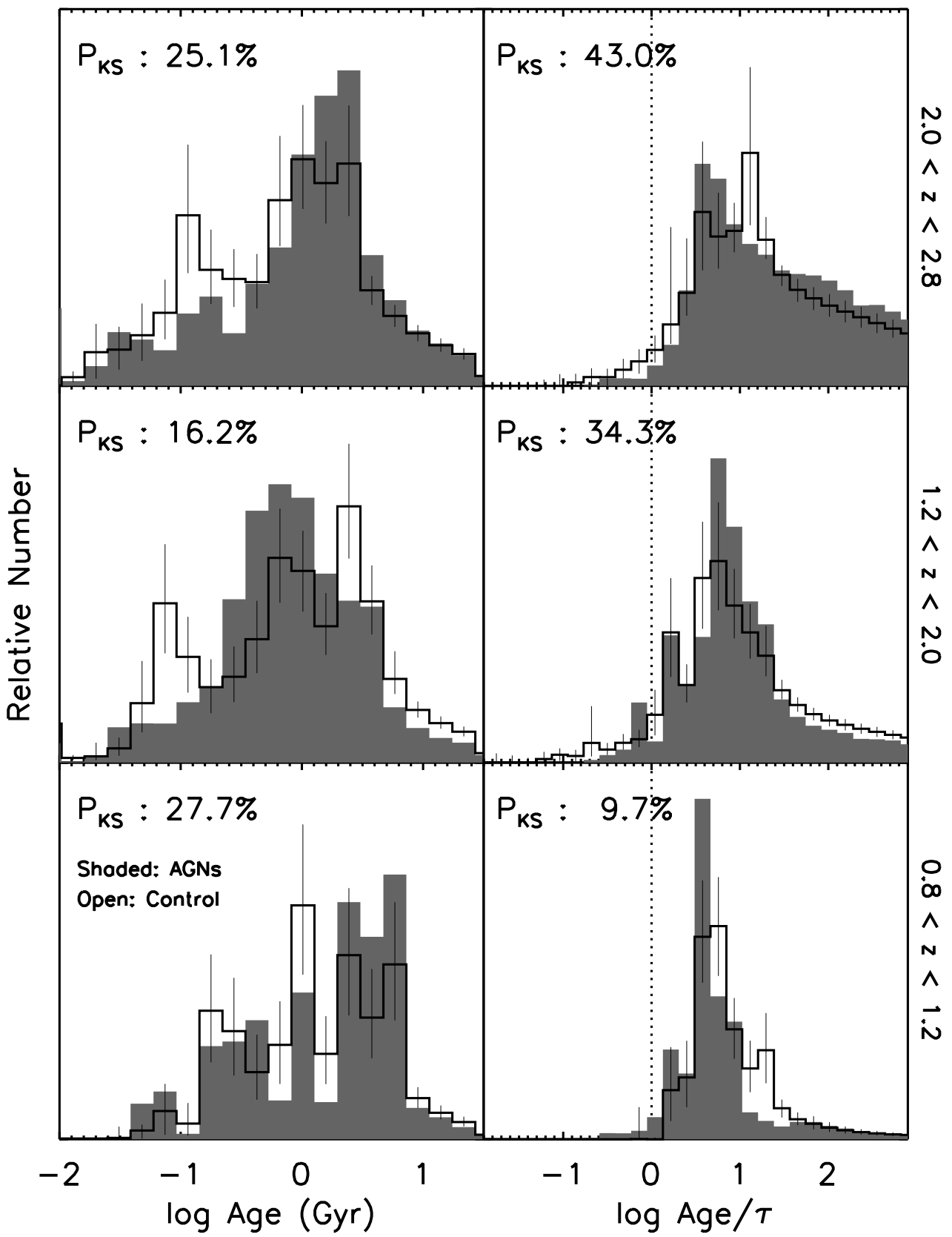

FIG. 18.— A comparison of the distributions of the light-weighted ages (left panels) and 'normalized ages' (right panels) of AGNs and control galaxies estimated from photometry in extended light apertures. AGN hosts (grey histograms) are compared to mass-matched inactive galaxies (open histograms) in three redshift bins, as indicated. Distributions have been regularized by a monte-carlo bootstrap procedure (§5.2). Error bars on the control galaxy histograms show the approximately 1σ variation in the distributions for sample sizes comparable to those of the AGN hosts. In each panel, the two-sided Kolmogorov-Smirnov probability P_{KS}, measured on the unregularized data, compares the similarity of the two distributions.

lar light in a large sample of AGN hosts in the X-ray luminosity range log $L_{2\text{-}10}$=42-44.5 erg s^{-1}.

Consistent with earlier studies, X-ray selected AGNs are found to reside in galaxies that are significantly more massive than the general field galaxy population. The typical stellar mass of AGN hosts is log $M_* \sim 10.5$ and it changes very little (less than a factor of 3) towards high redshifts. This suggests that low- to intermediate-luminosity AGNs reside in hosts of a characteristic stellar mass over a large range in redshift.

In keeping with their high stellar masses, AGN hosts are more likely to be found in galaxies with red or intermediate colors, compared to the general population of field galaxies. To account for covariances in galaxy properties that are a strong function of stellar mass, we make a detailed comparison of the colors, color gradients and SFHs of AGN hosts only to a mass-matched comparison sample of inactive galaxies.

We find that, to first order, AGN hosts at all redshifts have basic photometric properties – rest-frame colors, extinctions and color gradients – that are similar to inactive galaxies of the same total stellar mass. AGN hosts get considerably bluer and more compact towards higher redshifts, but this evolution is consistent with the changes seen in the inactive galaxy population as well. In addition, both AGNs and inactive galaxies show typically old stellar populations (ages $\gtrsim 1$ Gyr) and are better fit by models with a declining SFH at all redshifts (though the fraction of galaxies with flat or rising SFHs increases with redshift). The characteristic age of AGNs is long compared to the timescale of SF (i.e, τ for exponentially declining SF models). In essence, low- to moderate-luminosity AGNs are found in relatively normal massive galaxies at all redshifts to $z = 3$.

A closer examination though reveals small, second-order differences. Perhaps the most important one is that the characteristic (or modal) color of AGN hosts galaxies is slightly bluer than that of mass-matched control galaxies. The offset is hard to tie down, but is typically around $0.15 - 0.3$ magnitudes in U-B, with the largest and most significant differences found at $z \sim 1$. Small differences are also seen when we consider the SFHs of these galaxies. At $z \sim 1$, AGNs show slightly shorter median 'normalized ages' – stellar age/τ – than inactive galaxies, implying that AGNs have a slightly higher tendency to have formed more of their stars recently. This may point to more recent star-formation in AGN hosts than galaxies of similar stellar mass. Most of these differences weaken at intermediate redshifts ($1.2 < z < 2.0$), where we have the best statistics for AGN hosts. However, the small size of the AGN sample at $z \sim 1$ (14 galaxies) prevents a strong conclusion to be made about these differences and possible evolution with redshift.

It is at high redshifts that we find the largest differences between AGNs and inactive galaxies. While the AGNs typically display bluer colors than mass-matched inactive galaxies, a population of very young, strongly star-forming galaxies is under-represented among the population of AGN hosts. However, we caution that the construction of even a careful mass-matched control sample at high redshifts starts to become difficult, due to the larger uncertainties of mass measurements at these redshifts and the strong evolution in the number density of blue galaxies, which leads to more blue galaxies contaminating the control sample that at lower redshifts. In addition, as we suggest in §7.4, redshift errors and the spectroscopic selection biases, which differ between AGNs and inactive galaxy samples, may lead to systematic effects at these highest redshifts and complicate the interpretation of any offsets.

There are minor differences between the nuclear colors of obscured/low-luminosity AGNs and inactive galaxies as well. AGNs tend to show bluer mean colors in their central kpc, and the excess blue light is loosely correlated with the luminosity of the AGN. Such an excess may result from either enhanced SF in the central kpc which co-evolves with the level of SMBH accretion, or, alternatively, light from the active nucleus scattered into the line-of-sight from dust and gas in the extended emission line regions of the AGNs. The change in the mean nuclear color of AGNs is roughly 0.2 mag over two orders of magnitude in X-ray luminosity. If the excess is proportional to the AGNs X-ray luminosity, this would suggest that, on average, about 2-3% of the light in the U-band in X-ray AGN with log $L_{2\text{-}10} \sim 42$ erg s^{-1}within the central kpc of an AGN host galaxy comes from processes related to accretion.

10.2. *Comparison to Previous Studies at $z \sim 1$*

Pierce et al. (2010) studied the relationship between AGN luminosity, obscuration and galaxy color using an approach very similar to this work, but concentrating on AGNs at redshifts in the range $0.2 < z < 1.2$. Like us, they find that luminous, unobscured AGNs typically show strong nuclear blue excesses and steep color gradients consistent with AGN contamination. In addition, they uncover a tendency for softer X-ray sources to reside in galaxies with blue outer colors, again similar to our result in §7.2.

This unexpected trend between AGN host colors and AGN obscuration is not easily understood with popular models of AGN fueling and feedback. In particular, it is quite opposite to the relationship one would expect if AGN were primarily fueled by major galaxy mergers (Hopkins et al. 2008), where the most obscured phase of an AGN's duty cycle is associated with the most active phase of star-formation during a merger, while, in contrast, the AGN is typically unobscured and visible in the optical and UV bands during the post-merger blowout, when the stellar population quickly evolves onto the Red Sequence. Pierce et al. (2010) suggest that the result is more consistent with alternative fueling models, such as those developed by Ciotti & Ostriker (2007), in which the AGN is fueled by stellar winds and mass-loss that settle to the nucleus, coeval with a strong nuclear starburst.

Another possible scenario is that the intrinsic shape of the X-ray emission from red and blue galaxies is different. AGN hosts span a large range in galaxy mass, color and morphology. Red galaxies tend to be more massive and gas-deficient compared to star-forming blue galaxies. They are expected to have more massive black holes (Häring & Rix 2004), and yet less gas to fuel luminous phases of SMBH accretion. Therefore, red quiescent galaxies may be expected to host AGNs with lower Eddington ratios, on average, compared to star-forming galaxies. If the accretion disk and X-ray properties of the AGN are dependent on Eddington ratio, such that

SMBHs that accrete at lower Eddington rates are in a harder spectral state, as suggested by some authors (e.g. Trump et al. 2011), the positive correlation between N_H and galaxy color may by a direct consequence of lower mean Eddington ratios among the most massive, red galaxies. Recent studies of the AGNs at $z \sim 1$ from the PRIMUS survey (Aird et al. 2011) suggest, however, that AGN accretion rates are not a function of galaxy stellar mass. Further work on the accretion properties of the rare massive red galaxies can test these ideas and should be possible with the current large area, deep X-ray surveys, such as in the COSMOS field.

10.3. *AGNs and the Transformation of Galaxies*

Several studies have suggested that the high frequency of AGN in the Green Valley is evidence of a close association between the quenching of star formation in galaxies and the feedback from active nuclei. According to this scenario, the energy output of the accreting SMBH couples with the gas in the disk of a star-forming blue cloud galaxy and either drives most of it out of the galactic potential, or, alternatively, heats it to a temperature beyond 10^6 K. At this point, the gas is too hot or too diffuse to cool back into the galaxy disk and the star-formation shuts down. The time-scale of AGN-driven quenching is short enough that the galaxy's light is dominated by an intermediate aged stellar population with colors typical of the Green Valley. The relative infrequency of Green Valley galaxies, reflected in the color-bimodality of the galaxy population, is a consequence of the rapidity of AGN-driven quenching. A similarity between the estimated time-scales of AGN activity and the time-scales needed to move a quenched galaxy onto the Red Sequence seems to imply a close association between the two processes (Schawinski et al. 2007; Bundy et al. 2008). (Schawinski et al. 2007) also find close associations between a population of local blue early-type galaxies and AGN activity, indicating that AGN may play a role in the quenching of ongoing star-formation in such systems.

However, an elevated fraction of AGNs in the Green Valley can also arise from a simple phenomenological explanation, which does not require a strong role for AGN feedback in the transformation of galaxies. Two key ingredients necessary for producing an AGN are a) fuel, in the form of relatively cold inter-stellar gas in the host galaxy, and b) a supermassive black hole. For an accreting black hole of a given mass to be detected at intermediate-to-high redshifts in a typical deep flux-limited X-ray survey, it either needs to have a high accretion rate (or Eddington ratio) or a high black hole mass, or both. Since massive black holes are typically found in galaxies with massive spheroids (e.g., Häring & Rix 2004), the detection rate of X-ray AGN will increase with bulge fraction and stellar mass, but to a point. The most massive galaxies at essentially all redshifts are almost always elliptical galaxies, which have hot haloes and are deficient in cold gas, due to heating in virial shocks Birnboim et al. (2007), feedback from radio jets (Best et al. 2006; Croton et al. 2006) or strong 'quasar mode' feedback during a possible earlier major merger episode (Di Matteo et al. 2005). Such systems are unlikely to host black holes that accrete significant quantities of cold gas. Therefore, in this picture, X-ray AGNs are preferentially found in galaxies with massive spheroids (and black holes), but also with disks which contain sufficient cold gas to keep up regular cycles of accretion. Such galaxies are typical of the Green Valley (Cassata et al. 2007). In this scenario, the prevalence of AGNs in galaxies with intermediate colors is solely a consequence of the necessary conditions for an accreting black hole to be detected in X-rays, coupled with the known relationships between SMBHs and spheroids (Tremaine et al. 2002; Kormendy et al. 2011), which is probably set during high accretion rate phases, such as through galaxy mergers (Hopkins et al. 2008). Considerable scatter in the location of AGNs in the color-mass diagram would be naturally expected, mostly towards redder galaxy colors, since some early-type galaxies are known to contain sizable amount of cold dusty nuclear gas (Ferrarese et al. 2006), possibly through settling of dense gas in hot atmospheres or mass loss from evolved stars. This is indeed observed for distant AGNs (Nandra et al. 2007; Brusa et al. 2009; Cardamone et al. 2010).

If indeed AGN hosts are indistinguishable from a population of massive inactive galaxies of the same stellar mass, this would support the latter scenario. Then, the characteristics of AGN hosts would be set not by the AGNs themselves, but by the strong dependence of galaxy properties on stellar mass, modulated by the conditions necessary to fuel SMBH accretion (massive bulge and gas-rich disk). On the other hand, if AGN hosts deviate from inactive galaxies of the same stellar mass in a systematic way, this could indicate that nuclear activity does in fact play a role in determining the gross properties of the hosts and lend support for a more intimate two-way connection between AGNs and their hosts.

Unfortunately, our study is somewhat inconclusive in this regard. We can say for certain that a large part of the typical properties of AGN hosts are set by their stellar mass, rather than the fact that they host an accreting SMBH. This is clear since AGNs for the most part are really quite similar to inactive galaxies of the same mass. This rules out any models that postulate strong differences between the AGN and normal galaxy population, for e.g., models that tie most nuclear activity to galaxy mergers or post-mergers. Such a result is consistent with recent studies that find that AGNs have very similar morphologies to inactive, mass-matched galaxies across the range of redshift we probe in this work (Cisternas et al. 2011; Kocevski et al. 2011).

On the other hand, we notice some differences at $z \sim 1$ – for e.g., the tendency for AGN hosts to have a narrow range in U-B color and have shorter normalized ages than inactive galaxies – which should not be strongly affected by systematics in the construction of a control sample. Therefore, we suggest that AGNs at lower redshift do differ slightly from inactive galaxies. They have a tendency towards older stellar ages, but a slightly higher fraction have formed stars more recently. These two apparently opposing results may be reconciled if AGN hosts have older formation times but broader SF timescales than inactive galaxies. In other words, they have formed a small fraction of stars more recently, possibly in association with the process that drives accretion.

At higher redshifts, these differences become less pronounced and more susceptible to systematics. Our in-

termediate redshift bin ($1.2 < z < 2.0$) has the best statistics, low incompleteness and stellar mass uncertainties that are not too severe. In this bin, we find that AGNs are most closely similar to inactive galaxies. The small differences we measure suggest a slightly elevated fraction of young stars among AGNs at these redshifts compared to inactive galaxies – again suggesting that recent star-formation may have occurred alongside or before the AGN phase. This is consistent with recent work on the FIR properties of the host galaxies of low and moderate luminosity AGNs (Mullaney et al. 2011; Santini et al. 2011).

If AGNs are no different from inactive galaxies, or associated with low levels of recent star-formation, then the importance of AGNs as mechanisms for driving the prompt transformation of galaxies from star-forming to quiescence may be overstated. Such models predict that AGNs are in galaxies with less recent SF, not more, since the phase of AGN activity leads to the immediate quenching of star-formation, while in galaxies without AGNs, star-formation can proceed unabated. However, a possible variation on this scenario may be able to reconcile our observations with a role for AGN feedback. If AGN activity is synchronized with star-formation phases, it is possible that feedback may effectively shorten the timescale of star-formation and therefore reduce the efficiency of star-formation in these massive galaxies. In such a scenario, AGN hosts contain signatures of recent star-formation because it is only in galaxies with such recent star-formation that AGNs have been triggered, possibly by the same process that triggered the formation of stars as well. Such processes could be, for e.g., minor mergers or satellite interactions, bar instabilities or the infall of fresh gas from the inter-galactic medium. The feedback from the active nucleus would then cut short a burst of star-formation that would have continued longer had the AGN not been present. In this way, by gradually eroding the duty cycle of star-formation in massive galaxies, AGNs may be able to play a role in their transformation.

10.4. *Evolution in the Relationship of AGN Hosts to Normal Galaxies?*

From a large study of the morphologies and colors of AGN hosts in the Galaxy Zoo survey, Schawinski et al. (2010) find that local AGNs satisfy a strong preference for the Green Valley, even when mass selection effects are taken into account. In particular, the most massive local galaxies are less likely to host AGNs compared to galaxies that have bluer colors and lower masses. A recent study of the properties of a hard X-ray selected BAT sample of AGNs (Koss et al. 2011), which span a luminosity range that is similar to the CDF-S 4 MSec sample, also find a similar result, while again accounting for stellar mass selection effects. Taken at face value, these studies suggest that local AGNs are still preferentially found in the Green Valley and may be more closely associated with a quenching galaxy population.

This contrasts considerably with what we find at $z > 1.5$, where AGN hosts have a similar spread in color and SFH as inactive galaxies of the same mass, and indeed are very common among the most massive systems at these redshifts. At $z \sim 1$, our results suggest a situation that is intermediate between these local studies and the properties of AGN hosts at higher redshift. If true, we may be witnessing a change with redshift of the relevant processes that relate substantial black hole accretion to the properties of the host galaxy. The high gas fractions and turbulent, clumpy gas disks seen among massive galaxies at $z \sim 2$ should allow more frequent and consistent inflow of gas to the central SMBH (Bournaud et al. 2011). Such processes will be able to occasionally fuel even more luminous phases, such as quasars, which require disruptive processes like major mergers to drive them at low redshifts. If so, the relative importance of major mergers as the triggers of major SMBH growth at high redshift will decline, while secular processes, such as turbulent accretion, will be more important. This may explain the change in the association between galaxies and AGN activity towards higher redshift: if secular inflow can fuel most AGNs at $z \sim 2$, all galaxies with such gas disks will be able to accrete significant quantities to be able to shine as an X-ray AGN. In this case, every massive galaxy is a candidate AGN host. At lower redshifts, only massive spiral galaxies, with enough gas in their disks, can fuel secular AGN phases, while a larger fraction of Seyfert activity is fueled in post-merger systems (Schawinski et al. 2010). This will naturally lead to an evolution in the make-up of AGN hosts towards higher redshifts.

A deeper understanding of the physics of feedback, from simulations (e.g, Debuhr et al. 2010) and observations of active galaxies across a range of scales, is crucial towards constraining whether, how, where and when AGNs play a part in altering the nature of their hosts. Our study allows us to rule out the importance of strong and prompt quenching in AGNs but weaker, longer lasting and more pervasive processes could still have an critical role in modulating the transformation of galaxies. In addition, we suggest that evolution in the principal mode of AGN fueling may be relevant in studies of AGN hosts with redshifts. As the CANDELS survey expands, we will be able to study ∼1000s of AGNs across a wide range of redshifts with this remarkable dataset and, hopefully, tease apart the various roles of galaxy mass, gas inflow, AGN luminosity and feedback in the evolution of active galaxies.

REFERENCES

Aird, J., Coil, A. L., Moustakas, J., et al. 2011, arXiv:1107.4368
Ammons, S.M., et al. 2011, submitted
Antonucci, R. 1993, ARA&A, 31, 473
Arnouts, S. et al. 2007, A&A, 476, 137
Baggett, S.M., et al. 2008, Proceedings of the SPIE, Volume 7021, pp. 70211Q-70211Q-11, eds.: Dorn, D., & Holland, A.
Baldry, I. K., Glazebrook, K., Brinkmann, J., Ivezić, Ž., Lupton, R. H., Nichol, R. C., & Szalay, A. S. 2004, ApJ, 600, 681
Bennert, N., Canalizo, G., Jungwiert, B., Stockton, A., Schweizer, F., Peng, C. Y., & Lacy, M. 2008, ApJ, 677, 846
Benson, A. J., Bower, R. G., Frenk, C. S., Lacey, C. G., Baugh, C. M., & Cole, S. 2003, ApJ, 599, 38
Best, P. N., Kaiser, C. R., Heckman, T. M., & Kauffmann, G. 2006, MNRAS, 368, L67
Birnboim, Y., Dekel, A., & Neistein, E. 2007, MNRAS, 380, 339
Bournaud, F., Dekel, A., Teyssier, R., et al. 2011, arXiv:1107.1483
Bower, R. G., Benson, A. J., Malbon, R., Helly, J. C., Frenk, C. S., Baugh, C. M., Cole, S., & Lacey, C. G. 2006, MNRAS, 370, 645
Brammer, G.B., van Dokkum, P.G., & Coppi, P. 2008, ApJ, 686, 1503

Brammer, G. B., et al. 2009, ApJ, 706, L173
Brusa, M., et al. 2009, A&A, 507, 1277
Bundy, K., et al. 2008, ApJ, 681, 931
Calzetti, D., Kinney, A. L., & Storchi-Bergmann, T. 1994, ApJ, 429, 582
Cardamone, C. N., Urry, C. M., Schawinski, K., Treister, E., Brammer, G., & Gawiser, E. 2010, ApJ, 721, L38
Cardelli, J. A., Clayton, G. C., & Mathis, J. S. 1989, ApJ, 345, 245
Cassata, P., Guzzo, L., Franceschini, A., et al. 2007, ApJS, 172, 270
Cattaneo, A., et al. 2009, Nature, 460, 213
Ceverino, D., Dekel, A., & Bournaud, F. 2010, MNRAS, 404, 2151
Ciotti, L., & Ostriker, J. P. 2007, ApJ, 665, 1038
Cisternas, M., et al. 2011, ApJ, 726, 57
Croton, D. J., et al. 2006, MNRAS, 365, 11
Davies, R. I., Müller Sánchez, F., Genzel, R., et al. 2007, ApJ, 671, 1388
Debuhr, J., Quataert, E., Ma, C.-P., & Hopkins, P. 2010, MNRAS, 406, L55
Di Matteo, T., Springel, V., & Hernquist, L. 2005, Nature, 433, 604
Ferrarese, L., & Merritt, D. 2000, ApJ, 539, L9
Ferrarese, L., Côté, P., Jordán, A., et al. 2006, ApJS, 164, 334
Gabor, J. M., et al. 2009, ApJ, 691, 705
Gebhardt, K., et al. 2000, ApJ, 539, L13
Giavalisco, M., et al. 2004, ApJ, 600, 93
Georgakakis, A., et al. 2009, MNRAS, 397, 623
Grogin, N., et al. 2005, ApJ, 627, 97
Grogin, N., et al. 2011, arXiv:1105.3753
Guo, Y., Giavalisco, M., Cassata, P., et al. 2011, ApJ, 735, 18
Guyon, O., Sanders, D. B., & Stockton, A. N. 2006, New Astronomy Reviews, 50, 748
Häring, N., & Rix, H.-W. 2004, ApJ, 604, L89
Hopkins, P. F., Hernquist, L., Cox, T. J., & Kereš, D. 2008, ApJS, 175, 356
Hook, R., Stoehr, F., & Krist, J., 2008, STECF, 44, 1
Hunt, L. K., & Malkan, M. A. 1999, ApJ, 516, 660
Kauffmann, G., et al. 2003, /mnras, 346, 105
Kocevski, D. D., Faber, S. M., Mozena, M., et al. 2011, arXiv:1109.2588
Koekemoer, A., Fruchter, A., Hook, R., & Hack, W. 2002, HST Calibration Workshop, p. 337
Koekemoer, A., et al. 2011, arXiv:1105.3754
Kormendy, J., Bender, R., & Cornell, M. E. 2011, Nature, 469, 374
Koss, M., Mushotzky, R., Veilleux, S., et al. 2011, ApJ, 739, 57
Laird, E. S., et al. 2009, ApJS, 180, 102
Luo, B., Brandt, W. N., Xue, Y. Q., et al. 2010, ApJS, 187, 560
Maraston, C. 2005, MNRAS, 362, 799
Maraston, C., Pforr, J., Renzini, A., Daddi, E., Dickinson, M., Cimatti, A., &Tonini, C. 2010, MNRAS, 407, 830
Marchesini, D., van Dokkum, P. G., Forster Schreiber, N. M., Franx, M., Labbé, I., & Wuyts, S. 2009, ApJ, 701, 1765
McGrath, E. J., Stockton, A., Canalizo, G., Iye, M., & Maihara, T. 2008, ApJ, 682, 303
McNamara, B. R., & Nulsen, P. E. J. 2007, ARA&A, 45, 117
Morganti, R., Tadhunter, C. N., & Oosterloo, T. A. 2005, A&A, 444, L9
Morrison, R., & McCammon, D. 1983, ApJ, 270, 119
Mullaney, J. R., et al. 2011, arXiv:1106.4284
Nandra, K., & Pounds, K. 1994, MNRAS, 268, 405
Nandra, K., et al. 2007, ApJ, 660, L11
Noeske, K. G., et al. 2007, ApJ, 660, L43
Peng et al. 2010, AJ, 139, 2097
Pierce, C. M., et al. 2007, ApJ, 660, L19
Pierce, C. M., et al. 2010, MNRAS, 405, 718
Pierce, C. M., Lotz, J. M., Salim, S., et al. 2010, MNRAS, 408, 139
Polletta, M., et al. 2007, ApJ, 663, 81
Pounds, K. A., Reeves, J. N., King, A. R., Page, K. L., O'Brien, P. T., & Turner, M. J. L. 2003, MNRAS, 345, 705
Rosario, D. J., Shields, G. A., Taylor, G. B., Salviander, S., & Smith, K. L. 2010, ApJ, 716, 131
Rupke, D., & Veilleux, S. 2011, ApJ, 729, 27
Salvato, M., et al. 2009, ApJ, 690, 1250
Salim, S., et al. 2005, ApJ, 619, 39
Sanchez, S., et al. 2004, ApJ, 614, 586
Santini, P. et al. 2011, A&A, submitted
Schawinski, K., Thomas, D., Sarzi, M., Maraston, C., Kaviraj, S., Joo, S.-J., Yi, S. K., & Silk, J. 2007, MNRAS, 382, 1415
Schawinski, K., Virani, S., Simmons, B., Urry, C. M., Treister, E., Kaviraj, S., & Kushkuley, B. 2009, ApJ, 692, L19
Schawinski, K., et al. 2010, ApJ, 711, 284
Somerville, R. S., Hopkins, P. F., Cox, T. J., Robertson, B. E., & Hernquist, L. 2008, MNRAS, 391, 481
Simmons, B., & Urry 2008, ApJ, 683, 644
Stockton, A., McGrath, E., Canalizo, G., Iye, M., & Maihara, T. 2008, ApJ, 672, 146
Sturm, E., et al. 2011, ApJ, 733, 16
Szokoly, G. P., Bergeron, J., Hasinger, G., et al. 2004, ApJS, 155, 271
Tadhunter, C. 2008, Mem. Soc. Astron. Italiana, 79, 1205
Taylor, E. N., Franx, M., van Dokkum, P. G., Bell, E. F., Brammer, G. B., Rudnick, G., Wuyts, S., Gawiser, E., Lira, P., Urry, C. M., & Rix, H.-W. 2009, ApJ, 694, 1171
Tremaine, S., et al. 2002, ApJ, 574, 740
Tresse, L., et al. 2007, A&A, 472, 403
Trump, J. R., Impey, C. D., Kelly, B. C., et al. 2011, ApJ, 733, 60
Trump, J. R., Weiner, B. J., Scarlata, C., et al. 2011, arXiv:1108.6075
van der Wel, A., et al. 2011, ApJ, 730, 38
Whittle, M. 1992, ApJS, 79, 49
Willmer, C. N. A., et al. 2006, ApJ, 647, 853
Windhorst, R., et al. 2011,/apjs,193, 27
Wuyts, S., Labbe, I., Forster Schreiber, N.M., Franx, M., Rudnick, G., Brammer, G.B., & van Dokkum, P.G. 2008, ApJ, 682, 985
Wyder, T., et al. 2007, ApJS, 173, 293
Xue, Y. Q., et al. 2010, ApJ, 720, 368

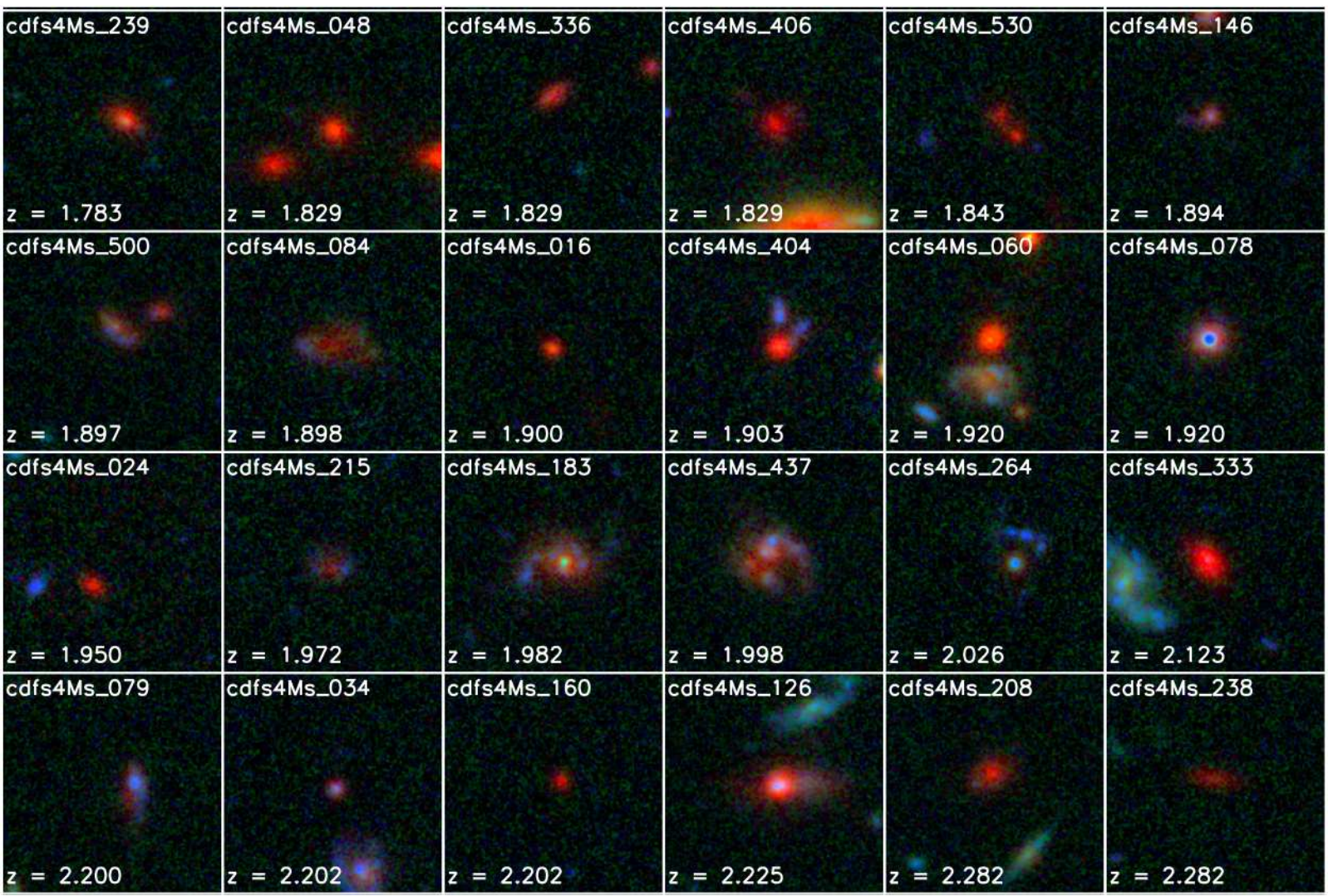
cdfs4Ms_239
z = 1.783
cdfs4Ms_048
z = 1.829
cdfs4Ms_336
z = 1.829
cdfs4Ms_406
z = 1.829
cdfs4Ms_530
z = 1.843
cdfs4Ms_146
z = 1.894
cdfs4Ms_500
z = 1.897
cdfs4Ms_084
z = 1.898
cdfs4Ms_016
z = 1.900
cdfs4Ms_404
z = 1.903
cdfs4Ms_060
z = 1.920
cdfs4Ms_078
z = 1.920
cdfs4Ms_024
z = 1.950
cdfs4Ms_215
z = 1.972
cdfs4Ms_183
z = 1.982
cdfs4Ms_437
z = 1.998
cdfs4Ms_264
z = 2.026
cdfs4Ms_333
z = 2.123
cdfs4Ms_079
z = 2.200
cdfs4Ms_034
z = 2.202
cdfs4Ms_160
z = 2.202
cdfs4Ms_126
z = 2.225
cdfs4Ms_208
z = 2.282
cdfs4Ms_238
z = 2.282

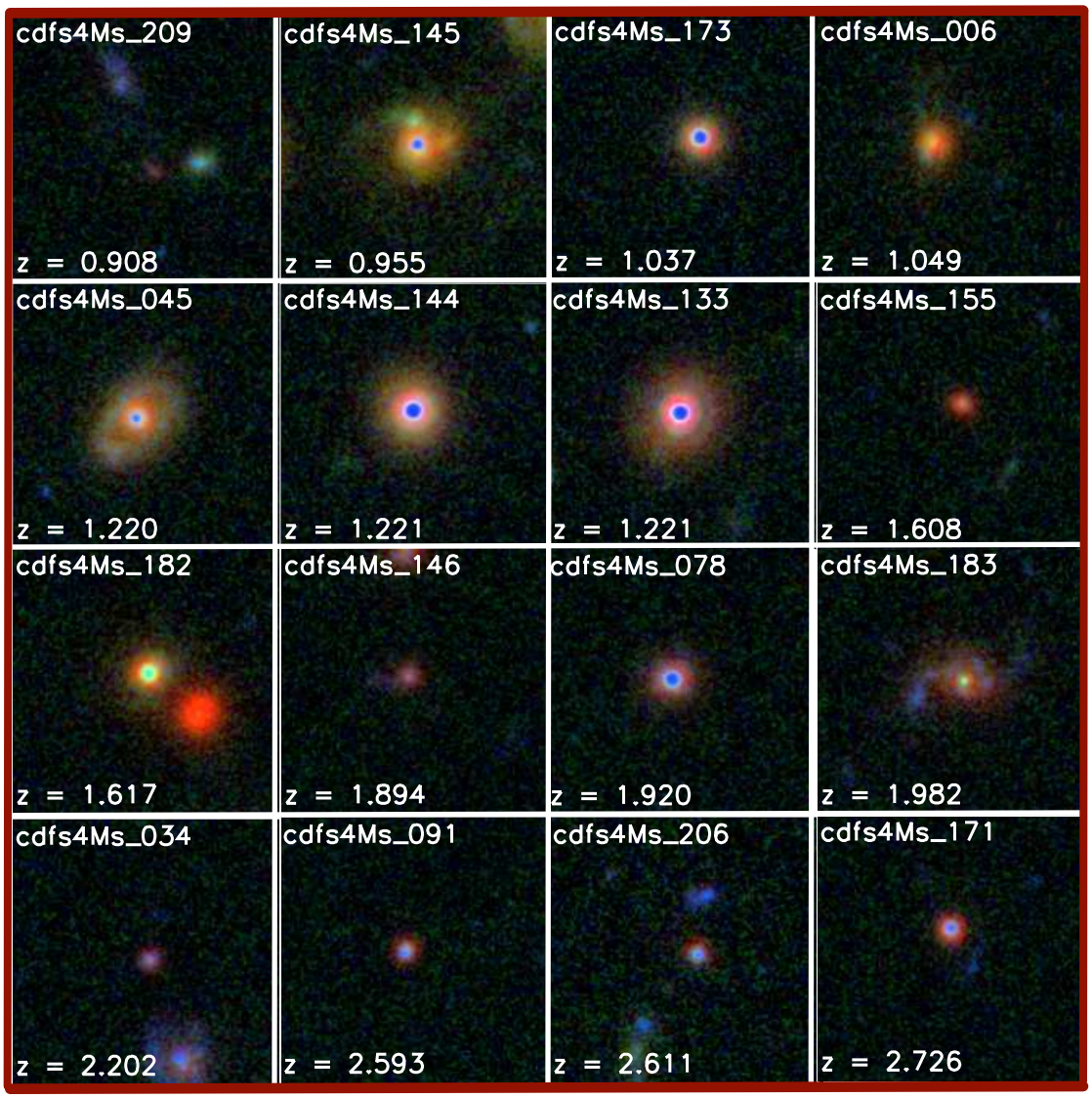
cdfs4Ms_209
z = 0.908
cdfs4Ms_145
z = 0.955
cdfs4Ms_173
z = 1.037
cdfs4Ms_006
z = 1.049
cdfs4Ms_045
z = 1.220
cdfs4Ms_144
z = 1.221
cdfs4Ms_133
z = 1.221
cdfs4Ms_155
z = 1.608
cdfs4Ms_182
z = 1.617
cdfs4Ms_146
z = 1.894
cdfs4Ms_078
z = 1.920
cdfs4Ms_183
z = 1.982
cdfs4Ms_034
z = 2.202
cdfs4Ms_091
z = 2.593
cdfs4Ms_206
z = 2.611
cdfs4Ms_171
z = 2.726